Master's thesis

NTNU
Norwegian University of Science and Technology
Faculty of Engineering
Department of Mechanical and Industrial Engineering

Lucas Emilio Guadiamos

High Performance AM Connecting Rod Design and Optimization

Master's thesis in Mechanical Engineering
Supervisor: Terje Rølvåg
June 2019

NTNU
Kunnskap for en bedre verden

Lucas Emilio Guadiamos

High Performance AM Connecting Rod Design and Optimization

Master's thesis in Mechanical Engineering
Supervisor: Terje Rølvåg
June 2019

Norwegian University of Science and Technology
Faculty of Engineering
Department of Mechanical and Industrial Engineering

NTNU
Norwegian University of
Science and Technology

Summary

The purpose of this Master Thesis was to optimize and design an AM high performance conrod for the Honda CRF250R motor. The optimization process was done using two separate methods, one including topology optimization in NX 12.0. The experimental research study looks at how internally hollow structures in the beam sections of connecting rods could help enhance their performance by giving a better load distribution in the beam as well as reducing weight. The proposed designs were benchmarked against the best performing MXRR conrod on the market today using four Key Performance Indicators (KPI's): Mass and Weight Distribution, Maximum Tension and Compression, Crank Speed and Acceleration and Maximum Von Mises stresses in Dynamic Simulation.

Once the designs were tested and approved by a static simulation in NX, a stiffness analysis was performed before they were analyzed dynamically in the Fedem Virtual Testbech, a virtual model of the CRF250R motor. After all simulations were completed the results were analyzed and compared.

All of the AM connecting rods showed an overall motor improvement both in maximum rpm output and in reducing the total weight of the motor assembly. With the right AM method applied in the production of these connecting rods the potential of these AM rods are undoubtedly present.

Sammendrag

Hensikten med denne masteroppgaven var å optimalisere og designe et AM høyytelsesråde til Hondas CRF250R motor. Optimaliseringsprosessen ble utført ved bruk av to forskjellige metoder der en av de inkluderte topologioptimalisering i NX 12.0. Oppgaven ser på hvordan internt hule strukturer i bjelkeseksjonene av råder kan bidra til å forbedre ytelsen, gjennom å gi en bedre belastningsfordeling i bjelken, samt å redusere vekten. De foreslåtte designene ble sammenlignet med og målt opp mot det beste MXRR-rådet på markedet i dag ved hjelp av fire Key Performance Indicators (KPI): Masse- og vektfordeling, maksimal strekk og kompresjon, krankhastighet og akselerasjon, og Maksimal Von Mises-spenning i dynamiske simuleringer.

Når designene var testet og godkjent av en statisk simulering i NX, ble det utført en stivhetsanalyse, før rådene ble analysert dynamisk i Fedem Virtual Testbech, en virtuell modell av CRF250R-motoren. Etter at alle simuleringene var fullført, ble resultatene analysert og sammenlignet.

Alle AM-rådene førte til forbedringer i motoren både når det gjaldt maksimal rpm og i reduksjon av totalvekten til motoren. Ved å bruke riktig AM-metode i produksjon av

rådene, er potensialet til AM-rådene utvilsomt til stede.

Table of Contents

List of Figures

Abbreviations

AM	=	Additive Manufacturing
BDT	=	Bottom Dead Center
CAD	=	Computer Aided Design
CAE	=	Computer Aided Engineering
Conrod	=	Connecting rod
DMLM	=	Direct Metal Laser Melting
DMLS	=	Direct Metal Laser Sintering
DOHC	=	Double Overhead Camshaft
EBM	=	Electron Beam Melting
FEM	=	Finite Element Modeling
FEA	=	Finite Element Analysis
FEDEM	=	Finite Element Dynamics in Elastic Mechanisms
FVTB	=	FEDEM Virtual Test Bench
HCF	=	High Cycle Fatigue
HIP	=	Hot Isostatic Pressing
KPI	=	Key Performance Indicator
MBS	=	Multi Body Simulation
OEM	=	Original Equipment Manufacturer
PBF	=	Powder Bed Fusion
SCBSV	=	Surface Curvature Based Size Variation
SFT	=	Small Feature Tolerance
SLM	=	Selective Laser Melting
TDC	=	Top Dead Center

Chapter 1

Introduction

This Master Thesis builds on the semester project *High Performance Connecting Rod Design And Optimization* by Lucas Emilio Guadiamos, and some of the content in this Thesis is a direct copy of that project paper.

The objective of the thesis is to design and optimize a high performance additive manufactured connecting rod. This will be done using a more traditional approach altering and making small adjustments to already existing designs, as well as utilizing topology optimization in NX to get some ”out-of-the-box”-design features. The new designed connecting rods will be benchmarked against MXRR’s top performing conrod for the CRF250R motor.

All new designs will be tested and evaluated in both NX and FEDEM, to get a static as well as a dynamic analysis of their performance. The results will be presented and discussed, and propositions towards improving the designs further will be given at the end of the report.

Chapter 2

Literature Review

Sections 2.1 to 2.4 are in their entirety copies of the semester project paper with the same name.

2.1 Strozzi et al. (2015)

The paper written by the italian professors focuses on the many different ways connecting rods tend to fail due to fatigue. They look at the forces distributed through the connecting rod during its life cycle, and their following stresses. The paper identifies the various locations of the critical sections of the connecting rod. The most critical sections identified by the study are shown in Figure 2.1. These areas will be taken into account when designing the new structure.

2.2 Vayssette et al. (2017)

This French publication looks at the effects of surface roughness on the high cycle fatigue life of Ti-6Al-4V parts obtained by different powder bed fusion processes. A combination of numerical simulations, torsion tests and SEM, is used to get an idea of the influence the surface roughness has on high cycle fatigue life.

2.3 Mower and Long (2015)

Mower and Long analyzed mechanical behavior of powder bed fusion manufactured alloys. These alloys included AlSi10Mg, Ti6Al4V, and the steels 316L and 17-4PH. They looked at the effect of post-processing to improve the fatigue strength, measured the surface roughness, examined the material microstructures, and used fractography to better understand their experiment. Mower and Long conclude that it is very possible to create AM specimens with similar or improved mechanical properties compared to machined

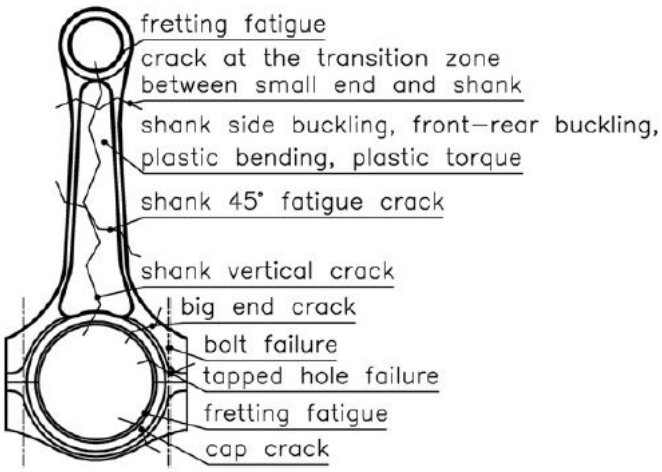

Figure 2.1: Most critical con-rod sections [Strozzi et al. (2015)].

specimens of the same materials.

2.4 Ek et al. (2016)

Ek et al. looks at the effects of the process parameters of EBM on the surface roughness. Ti6Al4V-ELI was the material used for the research. The study modifies a variety of factors iteratively, and looks at the effects of these modifications on three different specimens. The paper determines that the modification of the numbers of contours, the speed and current in the contours, as well as the contour offset, could be influential on the surface roughness.

2.5 Kuang-Hua (2015)

Chapter 4 in the book Design Theory and Methods Using CAD/CAE by Kuang-Hua discusses the topic of design sensitivity analysis, with a focus on linear elastic structures under static loading. In this chapter Kuang-Hua explains the theory behind topology optimization as well as the mathematics behind the softwares used in engineering today.

2.6 Xu et al. (2017)

The paper written by Xu et al. describes Selective Laser Melting(SLM) techniques that drastically improve the mechanical properties of Ti6Al4V compared to both other AM-processes and machined parts. The superior mechanical properties are achieved by turning unfavored α' martensite into lamellar $(\alpha + \beta)$ microstructures, using in-situ decompositions.

Chapter 3

Theory

3.1 Connecting rods

Parts of section 3.1 is taken from the semester project paper with the same name.

The connecting rod is what unites the piston to a crank or crankshaft. Together, these convert the alternating transverse motion from the piston to the rotational motion of the crankshaft [Strozzi et al. (2015)]. During the life span of an engine, the connecting rod is exposed to high-cycle fatigue loading, considering the forces induced by the gas explosions in the combustion chamber, as well as inertia forces. In this paper only symmetrical connecting rods will be looked at.

There are three different principal design groups when it comes to conrods. The two most common are the H-profile and the I-profile rods that can be seen in Figure 3.1a and 3.1b. The third design group is called oval rods.

(a) H-profile conrod. **(b)** I-profile conrod.

Figure 3.1: Common connecting rod profiles.

3.2 Additive Manufacturing

Section 3.2 is in its entirety a copy of the semester project paper with the same name.

The additive manufacturing processes that will be compared as possible manufacturing processes for the connecting rod are the powder bed fusion based processes, due to their relatively low cost and waste efficiency, as well as their large range of material options. Other processes such as Directed Energy Deposition and Binder Jetting, could have been looked at as well, but have been discarded due to their limitations.

3.2.1 Powder Bed Fusion (PBF)

Powder Bed Fusion processes are based on .STL-files as they create structures layer by layer, using a building platform, and a hopper containing metal powder. The platform is lowered incrementally as each layer is completed and a new layer of powder is laid across it. Different sintering or melting methods are utilized to connect powder to the previous layer, as will be described below.

Direct Metal Laser Sintering and Direct Metal Laser Melting

Direct Metal Laser Sintering (DMLS) uses a fiber-optic laser to partially melt the metal powder, connecting it to the previous layer. Lasers are also used in Direct Metal Laser Melting (DMLM) but opposed to DMLS, the metal powder is completely melted in the process, creating a density close to 100% of the original material. Due to their similarity to Selective Laser Melting, all these processes are often referred to as just SLM-processes.

Both DMLS and DMLM work with a variety of metals such as steel, aluminum alloys, and titanium, and are used both to created functional prototypes and finished products.

Electron Beam Melting (EBM)

Electron Beam Melting is, as DMLM, an AM process that completely melts the metal powder to connect it with the previous layers. It differs from DMLM as it uses a concentrated beam of electrons instead of lasers, to melt the metal particles together. This, alongside the desire to avoid any oxidation, is the reason why this process is done under vacuum.

EBM is first and foremost used in the production of titanium and superalloy parts for the medical and aerospace industry, due to its ability of printing intricate and complex designs. The EMB process can also provide similar or better mechanical properties than traditional production methods. In addition to this, the EBM process is 3-5 times faster than other AM processes [GE (2018)].

Mechanical properties of PBF manufactured parts

The surface roughness of PBF manufactured parts can be controlled by the thickness of the powder layers, with the possibility of getting an R_a of 5 μm for DMLM manufactured aluminum [Mower and Long (2015)], between 5 and 40 μm for DMLS manufactured titanium [Vayssette et al. (2017)], and around 4-5 μm for stainless steel [AlMangour and Yang

(2016)]. If you compare this to traditional machining methods, that can achieve a surface roughness around 1 μm, these are very good numbers, considering that the AM-methods are a lot less time consuming. This makes parts produced with DMLS and DMLM require very little, if any, post-processing.

Typical surface roughness for parts produced with Electron Beam Melting is between 20 and 50 μm [Ek et al. (2016)], which is a little higher than the DMLS and DMLM methods. Considering that, including post-processing, this method is far less time consuming than traditional production methods, the surface quality is still very acceptable.

In the study done by Vayssette et al. (2017), one can clearly see that the resistance to High Cycle Fatigue (HCF) is very dependent on the surface roughness. So much so that the nominal stresses for a life-time of 2×10^6, are more than halved for an SLM-process that is not postprocessed, compared to one that is.

Looking at the same study as for DMLS and DMLM processes, one can see that EBM-processes have an even greater difference between an un-postprocessed and a post-processed specimen. For the same life cycle as mentioned in the previous paragraph, an un-postprocessed specimen can only handle around a fourth of the nominal stress of a post-processed specimen. It is important to notice that this study was performed on Ti6Al4V-specimens, and that the results may vary for different materials, and AM methods applied.

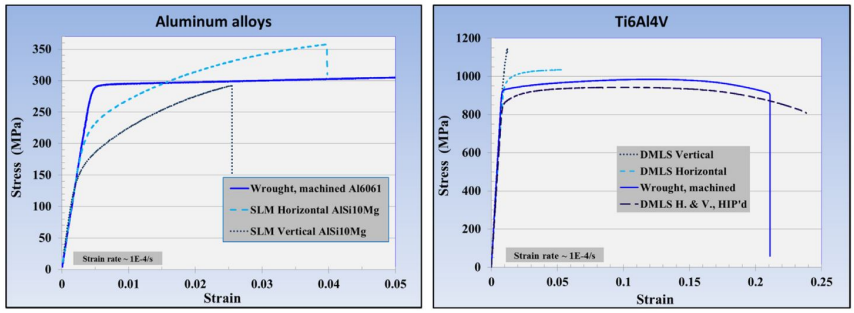

Figure 3.2: Mower and Long (2015): Stress-strain curve of Aluminum and Titanium alloys.

To see how these results vary, the study of Mower and Long (2015) and Xu et al. (2017) must be considered. The specimen fabrication and preparation is described in detail by both research papers and will not be discussed further in this thesis.

When evaluating the impacts of AM on the different alloys one can see that for the aluminum alloys, the stress-strain curve shows almost a halving in yield stress, while the titanium alloy has an almost identical stress-strain curve compared to traditional machining. The biggest difference can be found in the aluminum alloy, where the specimens failed after strains of only 0.025 and 0.04 for vertically- and horizontally-grown specimens respectively. These stress-strain curves can be seen in Figure 3.2.

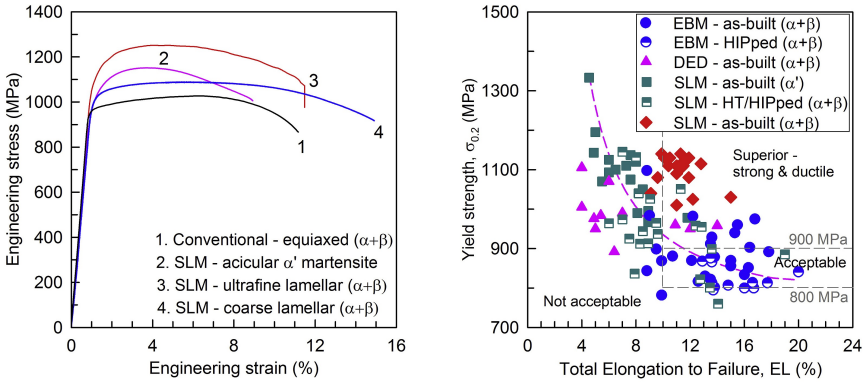

Figure 3.3: Xu et al. (2017): Stress-strain curve of superior Ti6Al4V.

Figure 3.3 shows the impact the altering of the SLM-process made by Xu et al. (2017) had on the Yield strength of the titanium alloy. Xu et al. achieved Yield strengths above 1000 MPa, while at the same time maintaining an acceptable ductility in the material. The maximum strain of around 15% for the coarse lamellar ($\alpha + \beta$) is three times higher than the maximum elongation achieved by Mower and Long (2015) for DMLS horizontal build of the same alloy. A HCF analysis of this super Ti6Al4V was not performed in the publication by Xu et al. (2017), and its lifetime under high cycle loading is therefore uncertain.

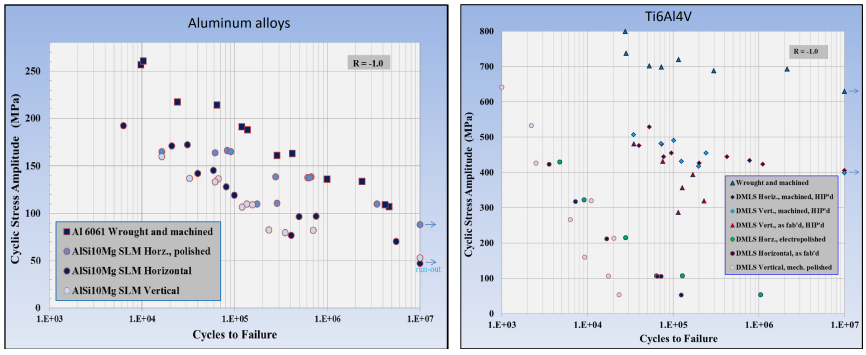

Figure 3.4: Mower and Long (2015): S-N curve of Aluminum and Titanium Alloys.

S-N curves for the aluminum alloy, see Figure 3.4, show a decrease of lifetime with a factor of about 10, and a stress tolerance 30% lower for the un-postprocessed AM specimens compared to the machined ones. For the titanium alloy, the S-N curves confirm what is discovered by Vayssette et al. (2017).; Life span is decreased dramatically. Exposing the specimens for HIP-treatment reduced this effect significantly.

For the steel specimens a different behavior was detected. The yield stress of the 316L stainless steel had increased as a consequence of AM, keeping an almost equal strain. The 17-4PH on the other hand showed fairly similar stress-strain curves between AM and machined specimens, even though the yield stress diminished, see Figure 3.5.

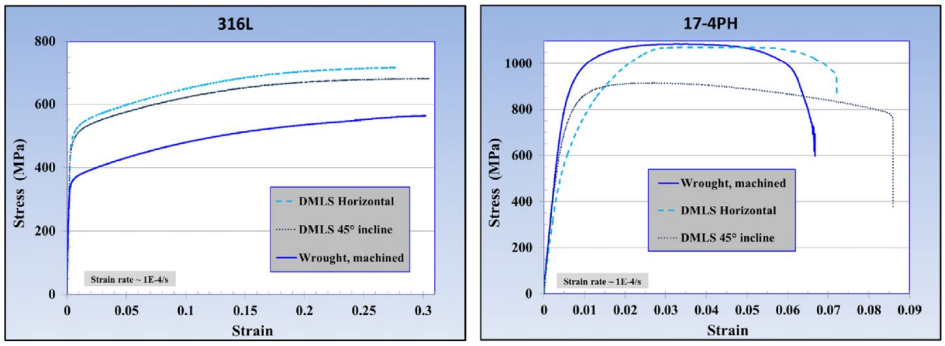

Figure 3.5: Mower and Long (2015): Stress-strain curve of Steels.

The S-N curves for the two steel alloys, seen in Figure 3.6, show that as for the titanium and aluminum alloys, 316L steel has a decrease in stress-life, but an HIP-treatment in this case had little impact on the lifetime of the specimen. AM 17-4PH on the other hand has a very similar lifetime compared to the machined specimens, as long as it's manufactured horizontally.

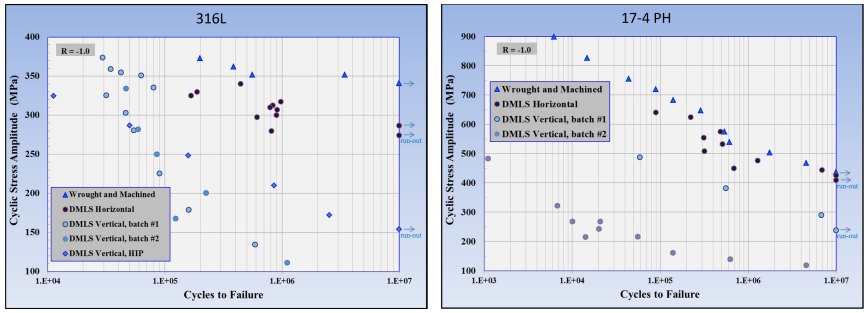

Figure 3.6: Mower and Long (2015): S-N curve of Steels.

3.3 FEDEM

Section 3.3 is in its entirety a copy of the semester project paper with the same name.

FEDEM is an acronym for Finite Element Dynamics in Elastic Mechanisms and is an analysis platform that enables complete post-processing and solving dynamic analyzes of 3D-models. Everything from stress and modal analysis to complete fatigue analyzes can be performed in FEDEM [Fedem Technology AS (2016)].

3.3.1 FEDEM Virtual Test Bench

Parts of this subsection is taken from the semester project with the same name as this thesis.

To simulate the forces and stresses that act on the connecting rod during a cycle, the FEDEM Virtual Test Bench for the Honda CRF250R motor is used. This has been developed by Terje Rølvåg and Matteo Bella, and is a representation of the Honda CRF250R motor with all its components with the ability to simulate dynamic motion and to perform detailed and accurate stress simulations of everything from the engines crankshaft to the piston and piston pins.

The FVTB has the ability to create exact predictions of the dynamic forces, stresses and displacements in the connecting rod during the life cycle of the motor. It does this by implementing Multi Body Simulation functions from the FEDEM software and combining them with a control system that simulates the effects of the electric starters, the ignition timing and power control [Rølvåg and Bella (2017)].

3.4 Siemens NX

Parts of Section 3.4 is taken from the semester project paper with the same name.

Siemens NX is a CAD/CAM/CAE software that will be utilized to mesh and assign material properties to the different connecting rods that are to be analyzed. The meshed parts are exported in to FEDEM in .nas-files and analyzed further.

3.4.1 CTETRA meshing in Siemens NX

There are several different mesh types available in Siemens NX. With regards to 3D-meshes CHEXA- and CTETRA-meshes are the ones that can be chosen from. When working on complex models, such as the conrods presented in this thesis, the CTETRA-mesh holds an advantage over the CHEXA-mesh in the way it handles sharp corners and edges. This is due to the elements shape which is tetraedrical, as opposed to the cuboidal shaped elements in the CHEXA-mesh.

Two different types of CTETRA-meshes can be used in NX, both with or without midside nodes. Siemens recommends to always apply the ten midside nodes [Siemens PLM Software Inc (2014)]

3.5 Topology Optimization

Topology optimization is a tool used to solve the engineering problem of material distribution within a limited design space. The main objective of topology optimization is to distribute the material in the best way possible, while still being able to handle the forces applied to the structural body [Kuang-Hua (2015)].

3.5.1 Topology Optimization in NX 12.0

Topology Optimization in NX 12.0 has been applied as a tool to optimize the design of the conrod. This is a fairly new add-on in NX, first introduced in NX 11.0, something that is visible when it comes to the limitation of freedom with regards to constraint features and load application. The workflow of this feature is illustrated in Figure 4.4.

Chapter 4

Experiment

4.1 Traditional workflow in NX

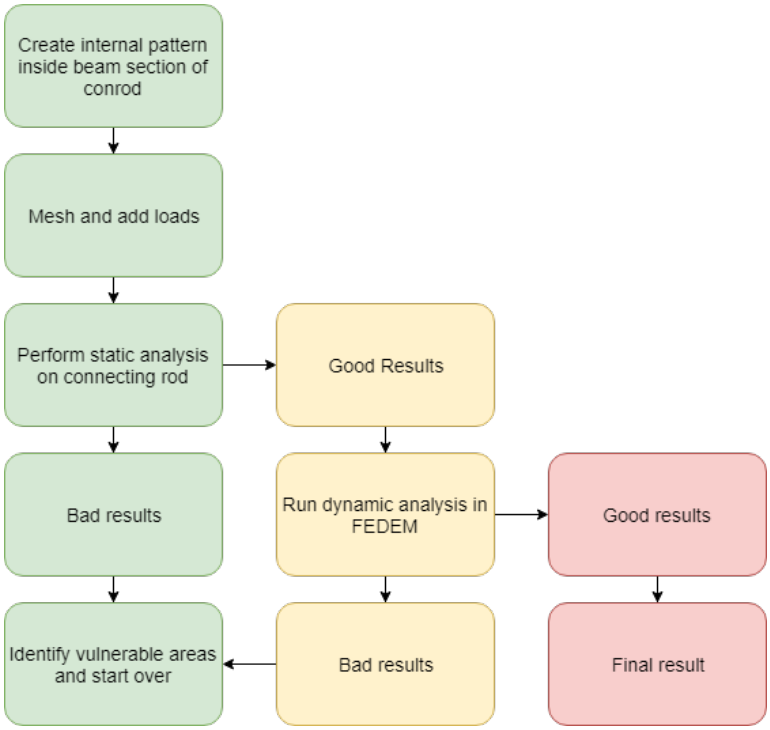

Figure 4.1: Traditional workflow using NX and FEDEM

To start with a traditional method of finding an optimal AM internal pattern was applied, the same method used in the semester project with the same name as this Thesis. The workflow of this method is illustrated in Figure 4.1.

This approach did provide some fascinating results, as will be discussed in section 5.1, but was very time demanding and the good results were based on previous results already obtained in the semester project. Topology optimization was therefore chosen as the next step in the process.

4.2 Workflow in NX using Topology Optimization

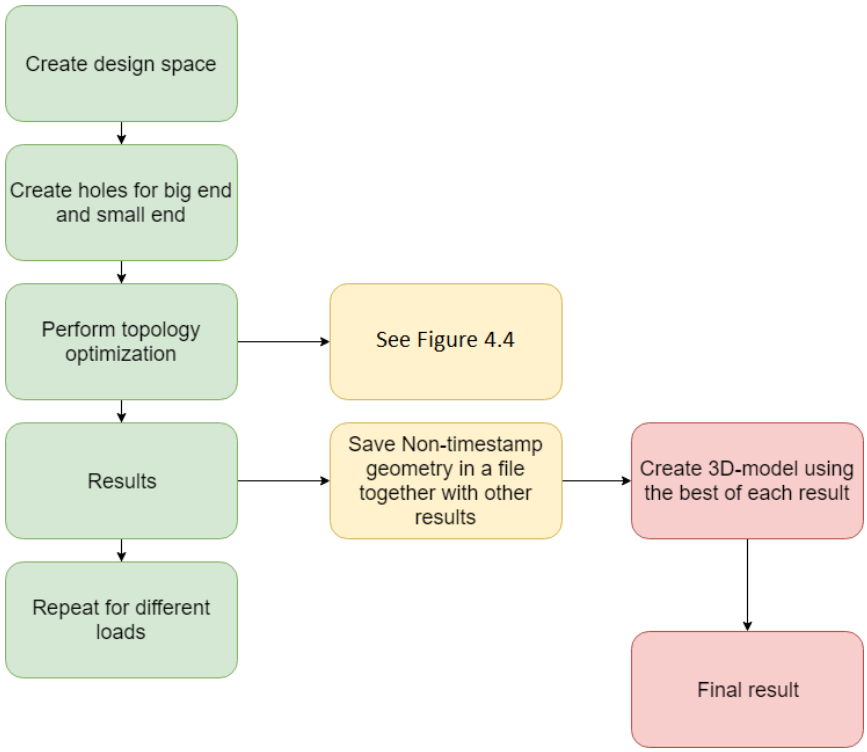

Figure 4.2: Flowchart NX using Topology Optimization

Given the limited constraint and load options in NX Topology Optimization, as well as limited computer power, the connecting rod topology optimization had to be performed through several steps, representing the different worst case scenarios the conrod goes through during a cycle. As can be seen in Sections 5.2.1, 5.2.2, 5.2.3 and 5.2.4, for this optimization, these steps included two stages of compression and two stages of tension.

The workflow in NX can be seen in Figure 4.2. The design space was created using the outer dimensions of the big end and the small end on the MXRR conrod the semester project paper is based on. With the holes created, the design space was cut in one quarter

given that planar symmetry was going to be used in the optimization. The design space was identical for all four cases presented later in the thesis and can be seen in Figure 4.3.

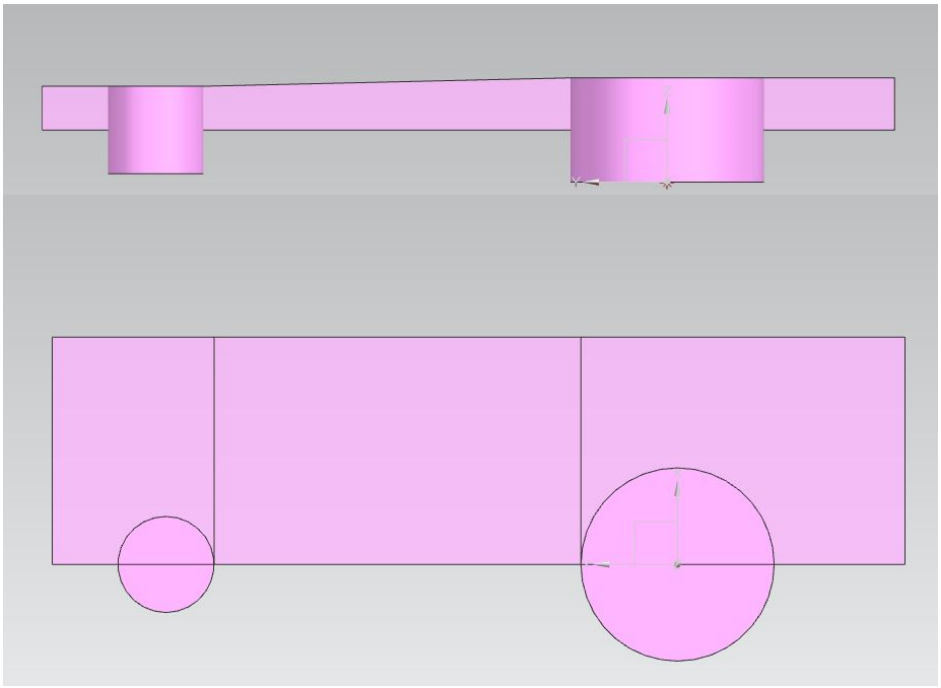

Figure 4.3: Design Space used in Topology Optimization

Combining the different Non-timestamp geometries into one solid body proved very difficult in NX, particularly when convergent modelling only worked on one out of four geometries. Meshing the results of the optimization directly only resulted in errors and failed meshes. A 3D-model was therefore created manually imitating the most organic features from each of the four results of the topology optimization. This is discussed further in section 5.3.

4.3 Workflow in Topology Optimization for NX 12.0

The workflow in the topology optimization tool is, as mentioned earlier, illustrated in Figure 4.4. The material used for the optimization was Ti6Al4V given the results found in Section 3.2. Due to limited computer power, no global loads were added to shorten simulation time. Manage Bodies will be discussed more in detail in Subsection 4.3.1 given its importance for the results.

The lowest resolution necessary to avoid the element sizes being larger than the offsets chosen was selected, and an optimization of minimizing volume subject to the materials safety factor was applied. This safety factor, Yield Stress on Maximum Von Mises Stress, was set to 1.0.

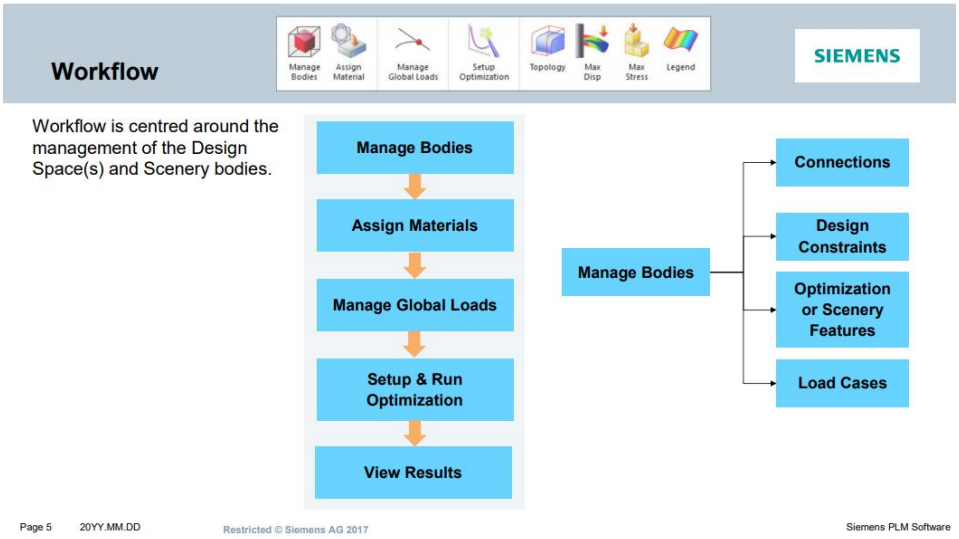

Figure 4.4: Siemens NX Topology Optimization Flowchart [Wills (2017)]

4.3.1 Manage Bodies

The Manage Bodies feature inside Topology Optimization contains, as seen in Figure 4.4, four areas of consideration. Since connections were not used to minimize simulation time, this feature will not be discussed further.

Design Constraints include planar symmetry, rotational symmetry, extrude along vector, draft, void fill, material spreading, overhang prevention and self-support. The first two are self explanatory.

Extrude along vector tells NX that the optimized part should be created as an extrude of a cross section in a certain vectorial direction. When using the draft constraint, the optimization will produce a topology that is suited for molding, casting or forging. An angle is assigned from which a straight pull-apart tool will have access to all surfaces. Void Fill prevents any internal voids from being created. Material spreading is used to hollow out, create thin walled structures or create strut like structures, depending on the level of 'spreading'. Overhang prevention prevents overhangs in a given direction. Self-supporting creates a geometry with no overhangs greater than those supported by the geometry itself. Multiple constraints can be applied, sorted in a user defined hierarchical order.

Optimization Features is where you assign properties to the different blocks, cylinders, spheres, holes, etc., created in your design space. As can be seen in Figure 4.5, several options need to be defined for each feature. If the features intersect each other in any way, the feature further up on the list will decide the outcome of the optimization.

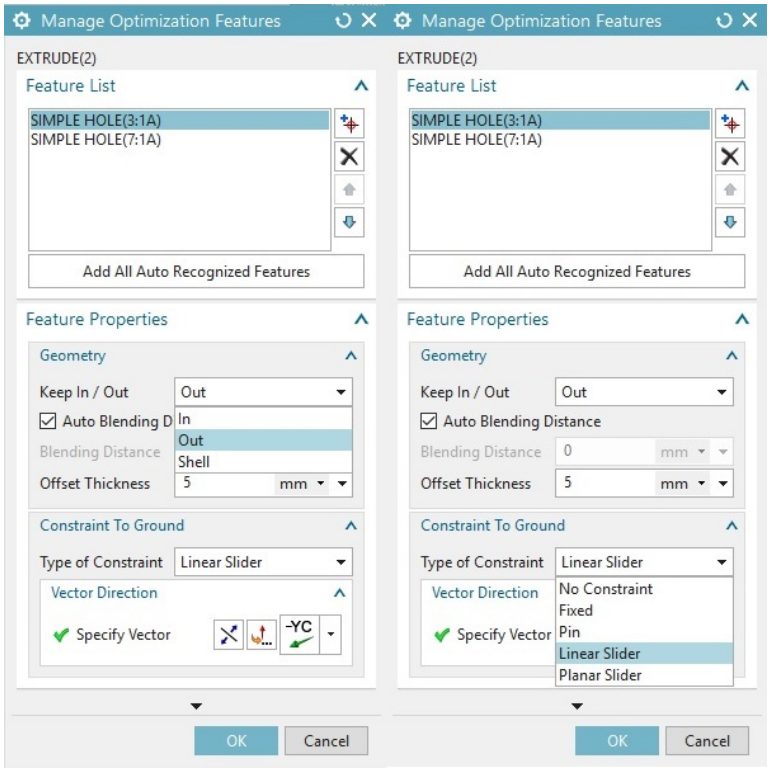

Figure 4.5: Optimization Features window in NX 12.0

In ”Keep In/Out” you select if the feature should be a part of the optimized geometry or not. The Shell option creates a shell around the geometry of the chosen feature on your feature list. An offset thickness can also be applied if desired. Next, Type of Constraint should be decided. It is possible to choose between several options as can be seen in Figure 4.5. ”No Constraint” and ”Fixed” are self explanatory. The ”Pin” constraint fixes the feature in all translational degrees of freedom, and rotation is only allowed about a specified vector. ”Linear Slider” and ”Planar Slider” are similar in the way that they only allow translational motion.The difference is that while ”Linear Slider” only allows translation along a specified vector, ”Planar Slider” allows translation as well as in-plane-rotation in a specified two dimensional plane.

Under ”Manage Load Cases” there are a few different loads that can be applied to the optimization features created in the previous step. These can be seen in Figure 4.6.

If ”Force” is chosen, the given load is distributed to the surface parallel to the specified vector. The ”Torque” option applies torque according to the right-hand rule and a specified vector. Pressure gives an even distribution normal to the chosen surface. A ”Bearing Load” is a distributed force applied on a cylindrical face or circular edge. It approximates the force distribution corresponding to a radial force transmitted between between two cylindrical surfaces or circular edges in contact with each other. ”Enforced Displacement” will allow the feature to be displaced with a given magnitude along a chosen vector.

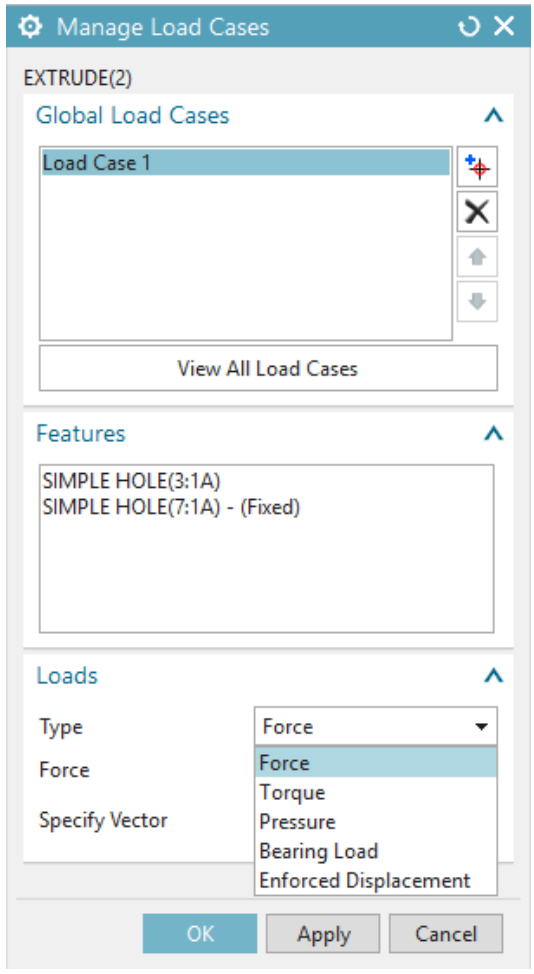

Figure 4.6: Manage Load cases window in NX 12.0

4.4 Moment of inertia; Stiffness analysis

The moment of inertia is directly correlated to the stiffness of a beam and a drop in moment of inertia about an axis will result in a reduced stiffness about the same axis for a given cross-section. A stiffness analysis was performed on the final results from both approaches of optimization to verify that the stiffness did not drop at unexpected places along the beam section.

The moment of inertia was obtained using the ”Edit Section” command in NX, copying the section curves from each section and analysing them using the ”Section Inertia Analysis” command. Furthermore the numbers were plotted in Excel. These results can be seen in Chapter 5.

4.5 The benchmark

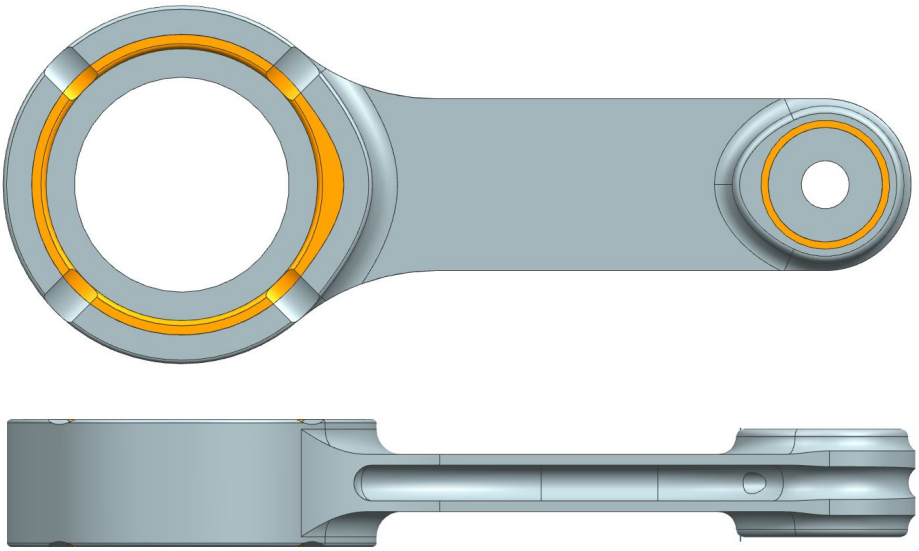

Figure 4.7: CRF250-MXRR-HSUP-O2 conrod

All the conrods created and tested will be benchmarked up against the CRF250-MXRR-HSUP-O2 conrod seen in Figure 4.7. This conrod is MXRR's highest performing connecting rod avaliable on the market today.

Figure 4.8 shows the stiffness analysis done on this connecting rod. From the figure a constant stiffness can be observed about the X-axis, or the critical bending axis, from section two to section twelve. The stiffness about the Z-axis is also quite constant throughout the beam. The lowest values of moment of inertia about the X- and Z-axis, 852.7 mm^4 and 3590 mm^4 respectively, will be used as comparison when evaluating the results of this thesis.

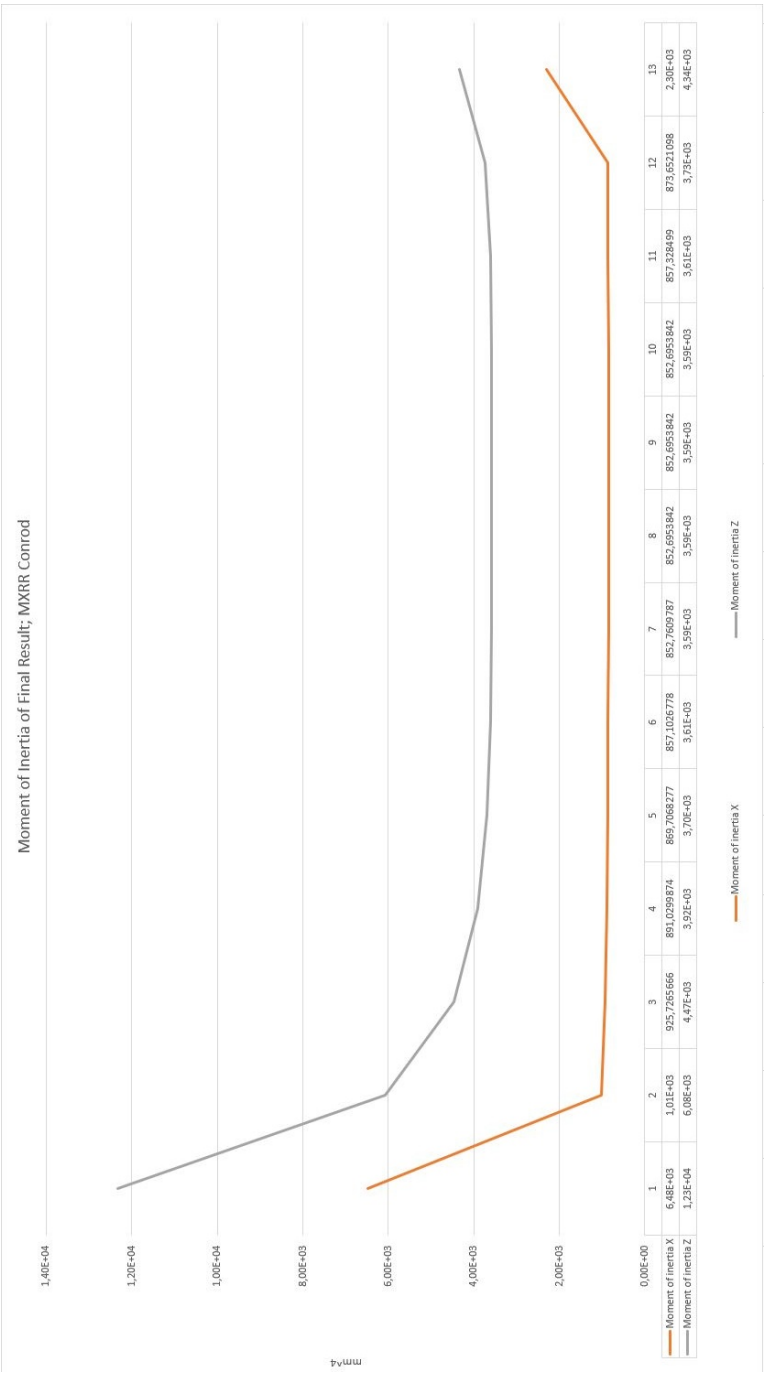

Figure 4.8: Moment of Inertia of beam section of MXRR conrod.

4.6 Key Performance Indicators (KPI's)

To be able to tell if a conrod is better than an other, key performance indicators have to be established in advance. Using some of the already established KPI's in the FVTB the conrods will be compared in 4 different KPI's elaborated in the following subsections.

4.6.1 KPI 1: Mass and Weight Distribution

Two very important factors when it comes to high performance motor parts is the mass and weight distribution of it. A part with minimum mass and a weight distribution such that the center of mass is as close to the center of rotation of the assembly as possible, is the most desirable. This reduces the effective crankshaft inertia forces and motor vibrations, while at the same time increasing acceleration and throttle response [Rølvåg and Bella (2017)].

4.6.2 KPI 2: Maximum Tension and Compression

This subsection is in its entirety a copy from the semester project with the same name as this thesis.

The connecting rod axial stresses are of great importance as they can be used to calculate the safety towards yielding and determine where the most critical points of the conrod are located. By comparing the different conrods in terms of this KPI one can easily find the best alternative towards axial stress resistance. The highest stresses are assumed to take place when the piston is at Top Dead Center(TDC) and full ignition of the fuel-air mixture takes place.

4.6.3 KPI 3: Crank Speed and Acceleration

This subsection is in its entirety a copy from the semester project with the same name as this thesis.

The MXRR Falicon rod has been designed and made to achieve an optimal crank speed, in regards to its mass and inertia influence on the crank. By comparing the crank speed and acceleration with the different design varieties, one can determine if the new designs are faster and have a smaller influence in decreasing the crank speed.

4.6.4 KPI 4: Maximum Von Mises stresses in Dynamic Simulation

The higher the maximum stresses are for a cyclic load the lower the life time of the component. It is therefore desired to lower the maximum stresses as much as possible. The conrod with the lowest Von Mises stress will have the longest lifetime, given material equality.

Chapter 5

Results

5.1 Results from traditional approach

Having seen in the semester project that a small honeycomb pattern would create too many small gatherings of high stress concentrations, a bigger internal pattern was introduced, as can be seen below in Figures 5.1, 5.2 and 5.3, and tested.

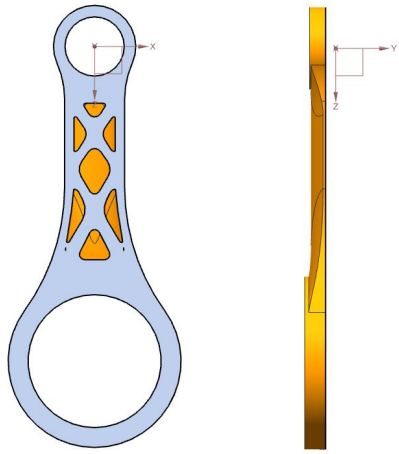

Figure 5.1: Cross-section of best result from traditional approach; back.

The pattern imitates trusses to get an ideal distribution of forces with two truss-sections divided, from left-to-right in the figures, by a beam going from the small end to the big end in the center of the beam. Both a beam section with one single truss-section from left-to-right, as well as a beam section with a truss-section including the beam from left-to-right was tested, but the results did not improve according to the increase of weight and these

designs were therefore discarded.

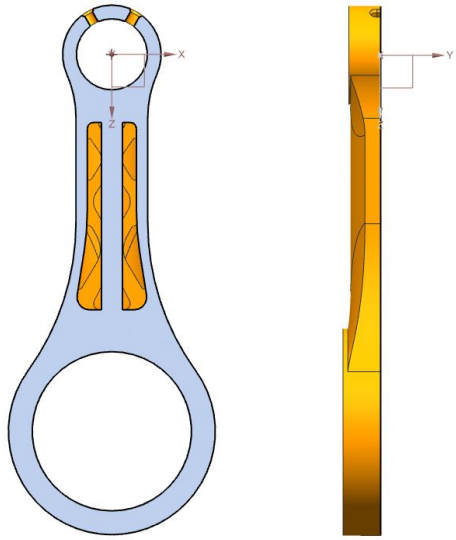

Figure 5.2: Cross-section of best result from traditional approach; Center.

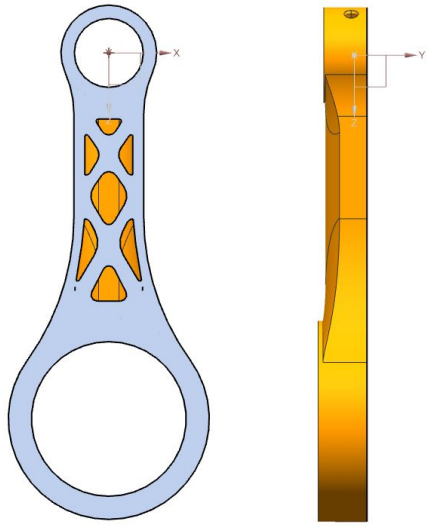

Figure 5.3: Cross-section of best result from traditional approach; Front.

5.1.1 Mechanical properties

```
Measurement Mass Properties

Displayed Mass Property Values
Volume                          = 27769.229516382 mm³
Area                            = 14505.633793057 mm²
Mass                            =    0.123017687 kg
Weight                          =    1.206391398 N
Radius of Gyration              =   37.466631465 mm
Center of Mass                  =   -0.000516493,    0.056482883,   61.572948907 mm
```

Figure 5.4: Mass properties of results of traditional approach

The mass properties of the traditional approach conrod can be seen in Figure 5.4, and are given with regards to a coordinate system with center in the small end and a positive Z-direction from small end to big end, as can be seen in Figure 5.5. The material selected is Ti6Al4V, as this was considered the most ideal for a low weight - high strength AM application.

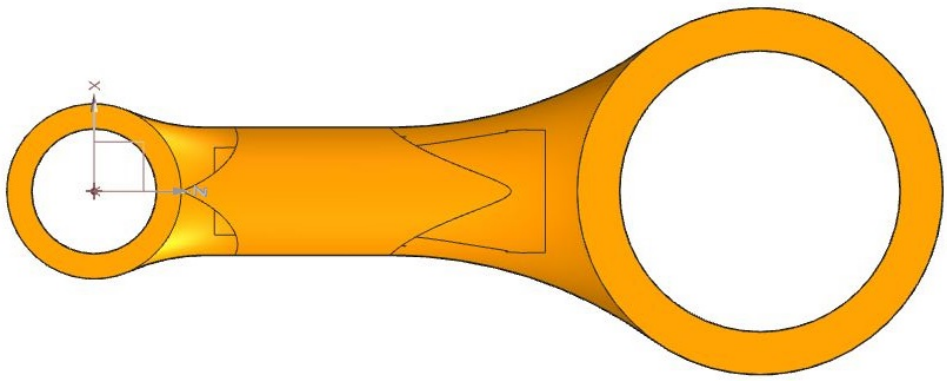

Figure 5.5: Coordinate system of traditional approach conrod.

5.1.2 Meshing; Results from traditional approach

The final result of the traditional approach was meshed with a CTETRA(10)-mesh due to the reasons explained in Subsection 3.4.1. Mesh size was sett to 2.5 mm, Surface Curvature Based Size Variation(SCBSV) was set to 50 % and the Small Feature Tolerance(SFT) was set to 10%. The mesh features selected are shown in Figure 5.6. This mesh gave a failed element fraction of less than 1% and almost no warning elements, something that was considered good enough for the further simulations.

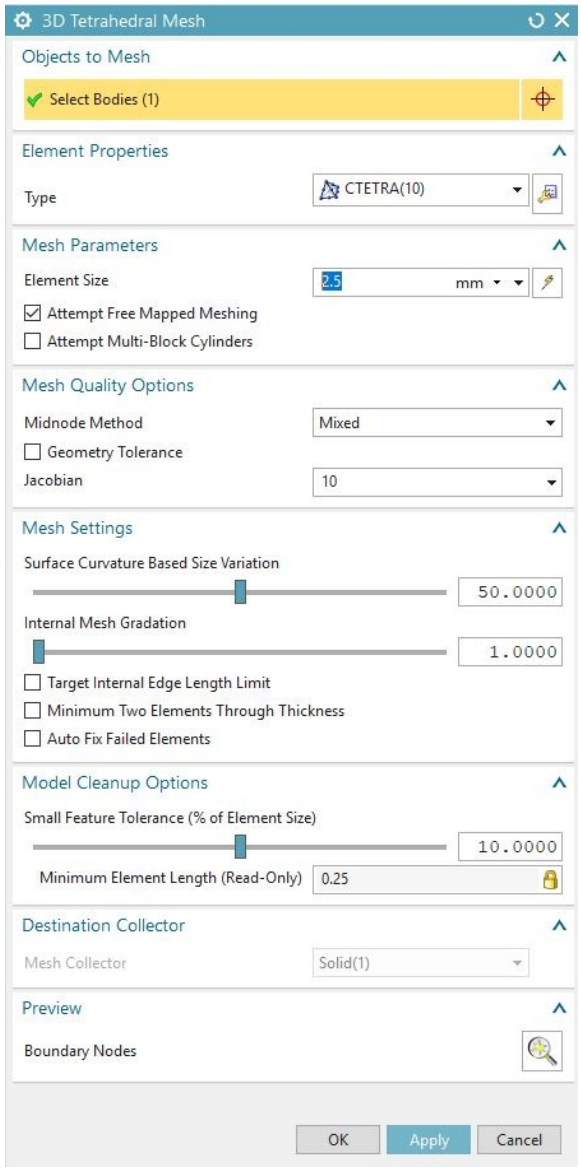

Figure 5.6: Mesh features; Results from Traditional Approach

5.1.3 Static analysis in NX; Traditional Approach Conrod

The Von Mises stresses are displayed in Figure 5.7, and the maximum stress of 802 MPa located in the small end will be lower once the piston pin is inserted. Maximum deformation is also found in the small end, displayed in Figure 5.8, with the value of 281 μm.

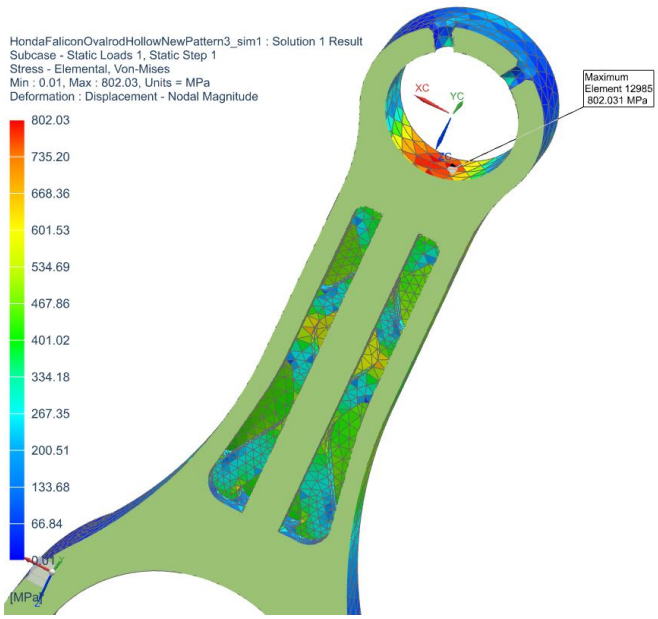

Figure 5.7: Von Mises stresses on the result of the traditional approach.

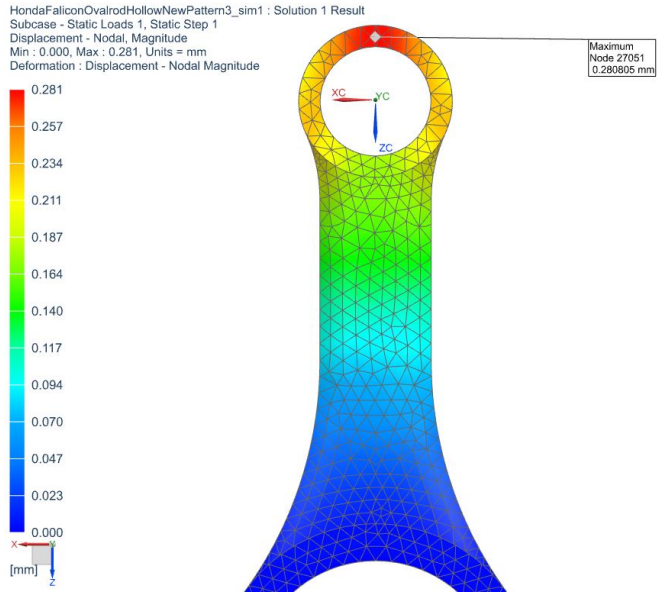

Figure 5.8: Deformation on the result of the traditional approach.

5.1.4 Stiffness Analysis

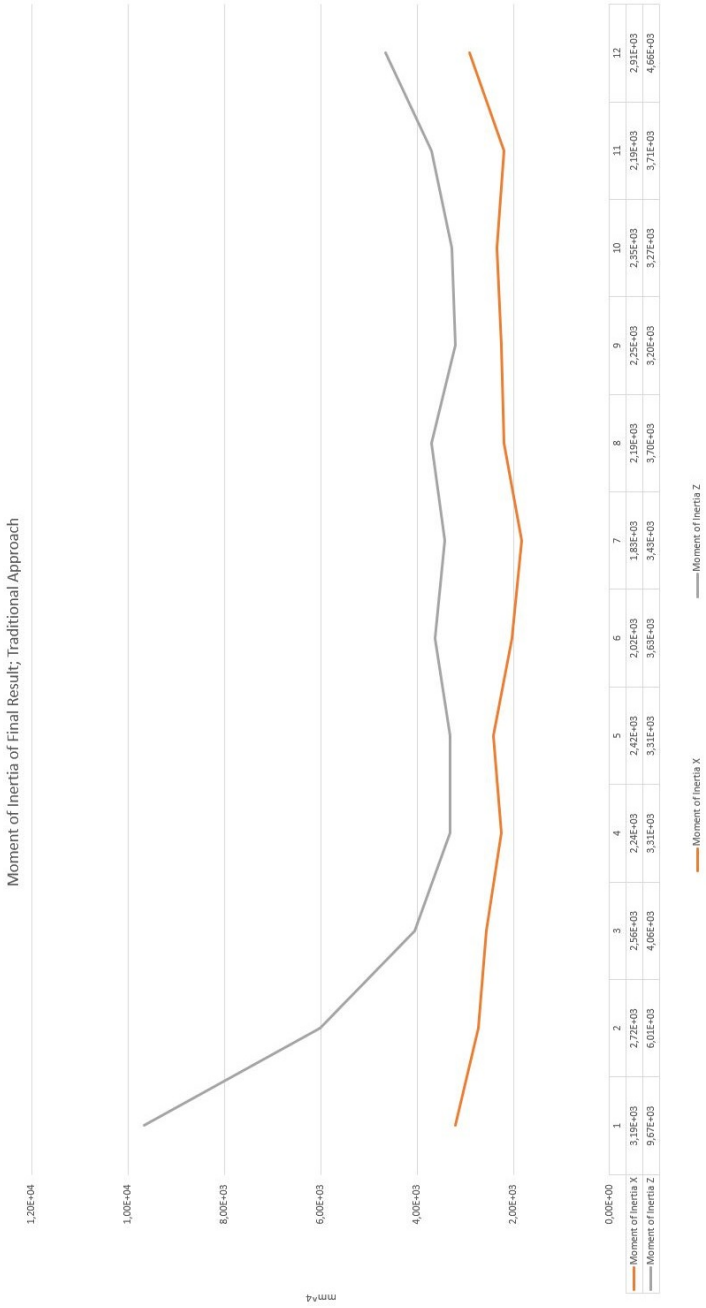

Figure 5.9: Moment of Inertia of beam section of the traditional approach.

For the stiffness analysis of the traditional approach conrod 13 cross-sections of the beam were looked at. As can be seen from Figure 5.9 the moment of inertia of the conrod is quite consistent in the whole beam, both in the X- and Z-direction. It can also be seen that the change in moment of inertia in both directions is fairly similar, indicating a symmetric change of area about both axis throughout the beam. The minimum values of moment of inertia can be read from the graph to be 1830 μm about the X-axis and 3200 μm about the Z-axis.

5.1.5 FEDEM Analysis of traditional approach

To see how the traditional approach conrod would perform inside an actual motor a dynamic analysis had to be excecuted. This was done in the FVTB mentioned in previous sections. Once inserted into the virtual motor block it would be benchmarked up against the MXRR conrod, sitting in the exact same motor block, the only difference being the conrod and the piston pin.

By using the mass properties (see Figure 5.4) a basic calculation distributing the total mass of the conrod in two point masses balanced at the center of mass was made. The results were plotted in the table of Figure 5.10 and the mass of the bob weight was calculated.

The bob weights are used in the FVTB to balance out the rotating masses during a full cycle, and can be seen as two small green coordinate systems in the bottom of the crankshaft on Figure 5.11. The figure shows the conrod inside the FVTB next to the MXRR conrod, and the internal pattern is also visible here.

TradAppFinal		
MXRR	big end	small end
Bearing	39	
RodWeight	84,17	
Oil etc	5	
Piston Pin		27
Piston		158
RodWeight		38,85
Factor		0,28
BobWeight	190,848	
Balance	103,3	
per node	51,6	

TradAppFinal weight	123,02
% small end	32
% big end	68

Figure 5.10: Calculation of Bob weights for FVTB.

Figure 5.12 shows the timing of the maximum piston force applied to the conrod. The conrod sits inside an Original Equipment Manufacturer(OEM) motor block and the piston is therefore referred to as an OEM piston on the graph. As can be seen from the graph the maximum force is around 54.7 kN and occurs around 1.51025 seconds. It's around this time the stresses shown in Figure 5.15 are recovered in the solver.

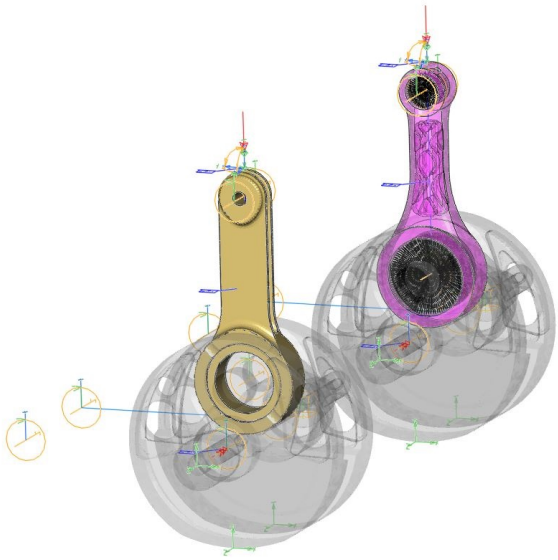

Figure 5.11: Conrod in FVTB next to MXRR conrod.

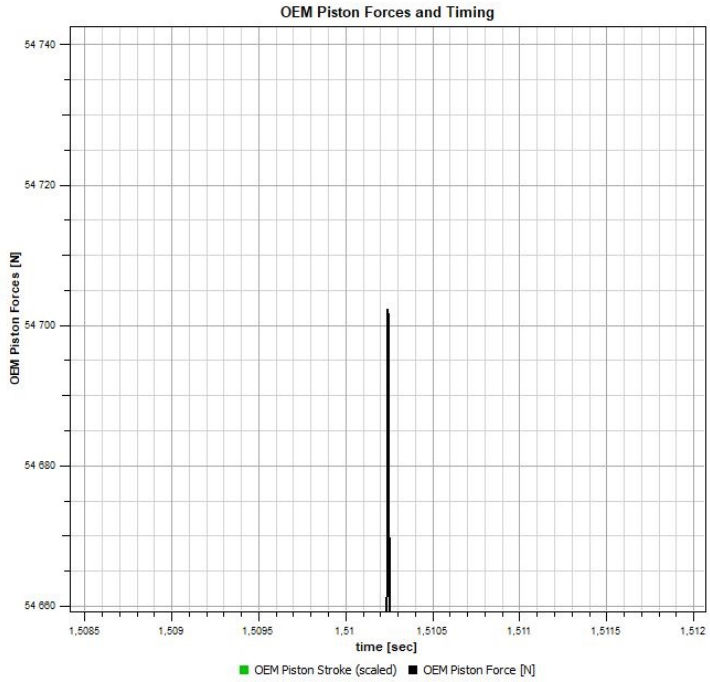

Figure 5.12: Maximum piston force applied to the conrod.

The traditional approach conrods maximum compression is displayed in Figure 5.13. As the figure shows, the maximum axial deflection of the traditional approach conrod is around 165 μm, far less than the deflection of the MXRR conrod at around 270 μm. This shows that the traditional approach conrod has a greater axial stiffness than the MXRR conrod.

This can also be seen on the strain by comparing the strain occuring at around 1.515 seconds to the strain in the MXRR rod at around 1.509 seconds. It's at around half the amount of its adversary.

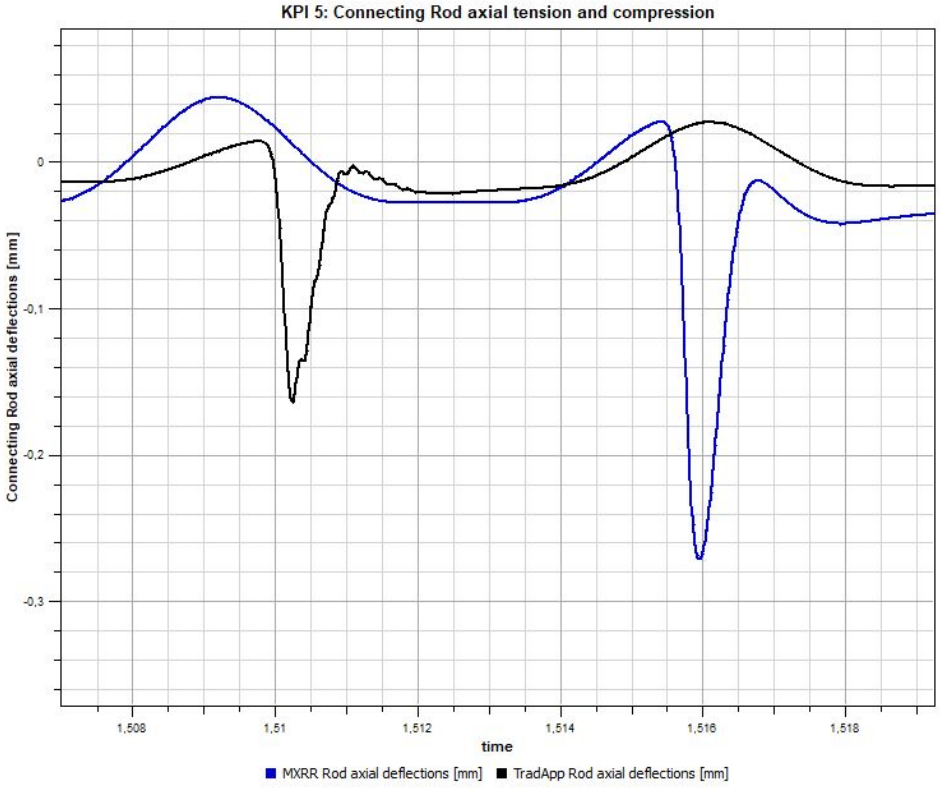

Figure 5.13: Maximum axial deformation in the traditional approach conrod compared to the maximum axial deflection in the MXRR conrod.

The maximum crank speed and acceleration is displayed in Figure 5.14. The black line in the graph indicates the crank speed achieved using the traditional approach conrod. Due to the low weight of the conrod the crank is able to achieve a maximum rpm around 500 rpm higher than for the crank with the MXRR conrod, applying the exact same forces on both systems.

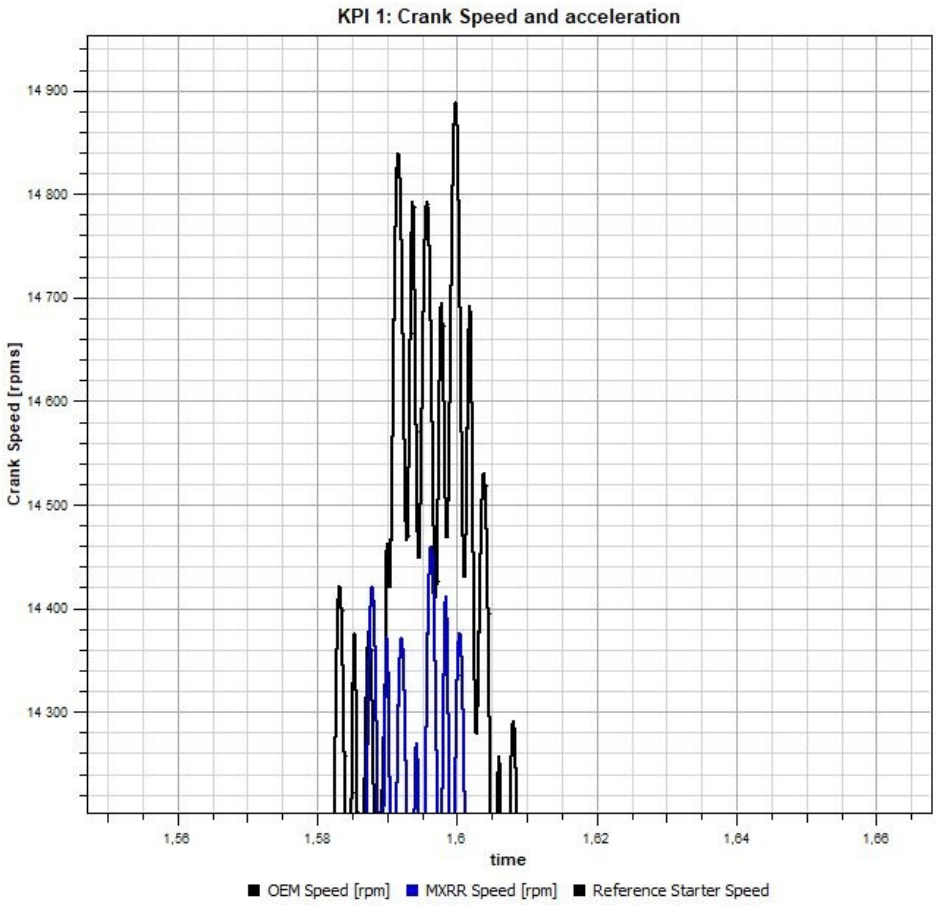

Figure 5.14: Maximum crank speed achieved with the traditional approach conrod.

Figure 5.15 displays the stress distribution on the conrod at the maximum piston force exposure. At first glance stresses above 600 MPa seem to be absent, but FEDEM indicates maximum stresses at 882.4 MPa at this instant. This can be seen in the top left corner of the figure. A quick look at Figure 5.16 shows that the maximum stress concentrations are, as expected, no longer present in the same place as they acted in the static analysis.

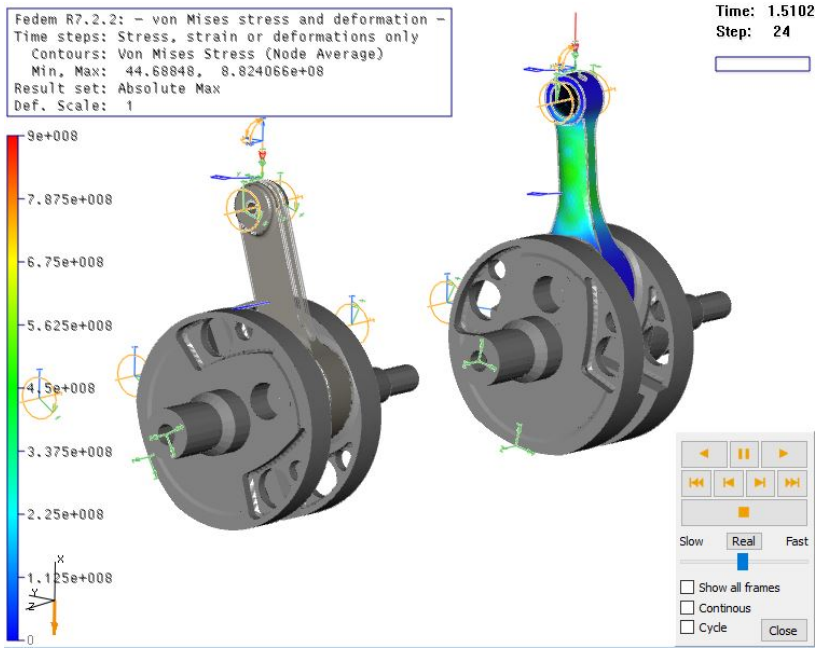

Figure 5.15: Von Mises stress on the results of the traditional approach conrod displayed in the FVTB.

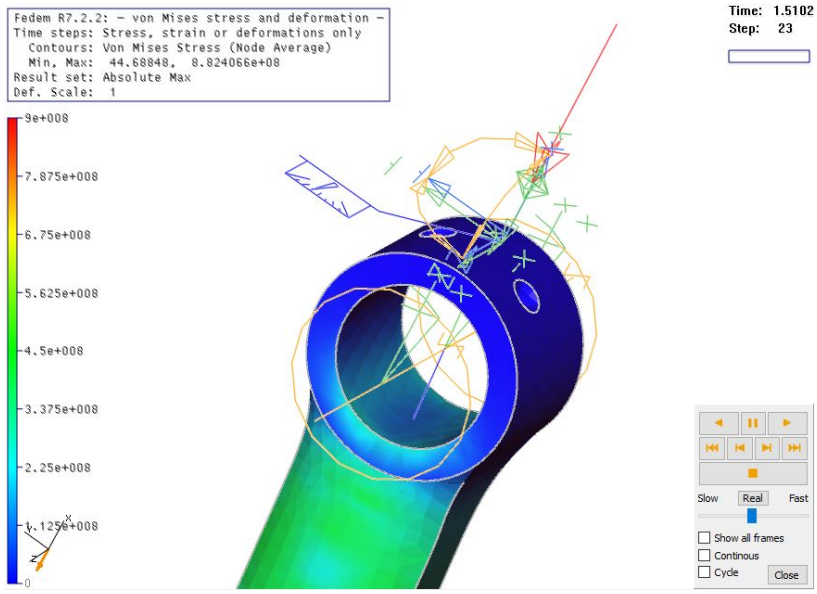

Figure 5.16: Von Mises stress on the results of the traditional approach conrod small end.

5.2 Topology Optimization Output

In all four cases below the bearing load applied had a value of 60 kN with an angular radius of 180°, as well as planar symmetry about the XY-plane and the YZ-plane to ensure a symmetric result. Material spreading was tested at different settings to evaluate the impact it had on the result.

The reference coordinate system used in all subsections below is the one seen in Figure 5.17, with the Y-axis going along the beam section with a positive direction from big end to small end. The Z-axis conincides to the center axis of the big end, and the X-axis is perpendicular on the two.

5.2.1 Compression; Fixed Big End

In the first case, displayed in Figure 5.17, the bearing force was placed in the simple hole constraining the small end. The force vector pointed in the negative Y-direction. Material spreading was set to 50.

As can be seen from Figure 5.17 the result contains several hollow sections resulting in a fairly organic structure. Given that the big end is fixed the program will acknowledge it as infinitely stiff, hence the thin walled result at the big end. This is also why the program considers it acceptable to keep only the centrally placed material above the big end. This would in reality lead to stress concentrations far greater than the yield stress of the material, causing the connecting rod to yield and fail.

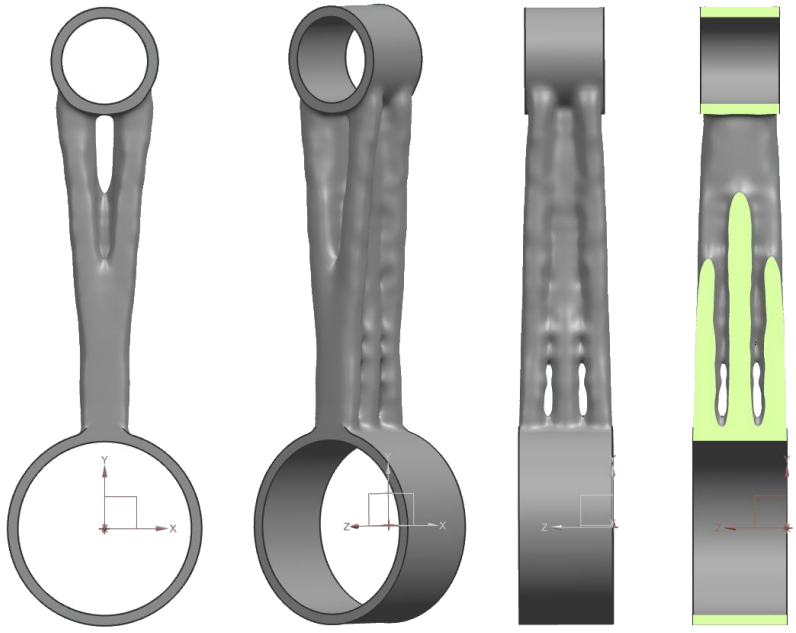

Figure 5.17: Best results from topology optimization, compression with fixed big end.

5.2.2 Compression; Fixed Small End

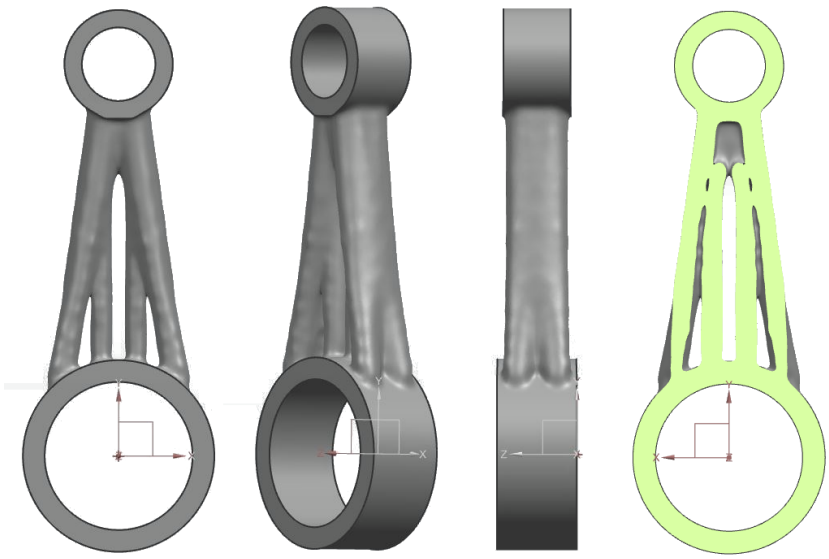

Figure 5.18: Best results from topology optimization, compression with fixed small end.

In the second compression case the force was applied in the simple hole constraining the big end while the small end was fixed. The force vector went in the positive Y-direction and material spreading was set to 50 as in the first case. The result is displayed in Figure 5.18.

As can be seen from the figure a wider cross-section closer to the big end has been implemented by the software to compensate for the force distribution. This result, being an inverted version of the result in Figure 5.17, shows a certain consistency in the software while at the same time underlining what was mentioned previously; the fixed geometrical constraint is considered infinitely stiff.

5.2.3 Tension; Fixed Big End

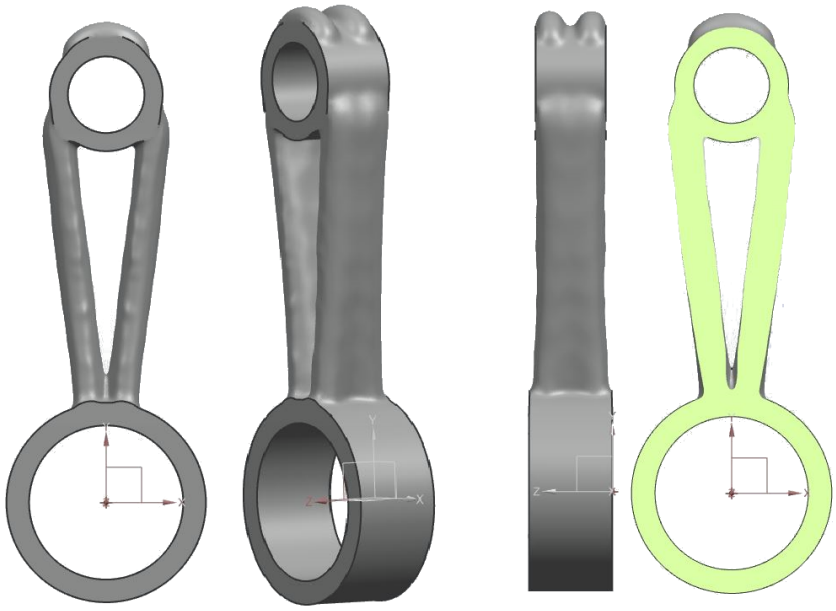

Figure 5.19: Best results from topology optimization, tension with fixed big end.

Figure 5.19 shows the best result of the tension optimization with fixed big end. The bearing load was applied in the small end in a positive Y-direction and in this case material spreading was set to 30.

The similarities to the result in section 5.2.1 are noticeable. In both cases a form of triangulation of the beam section is shown as an optimized geometry for the load case, suggesting that this would be a reasonable feature to keep. But here, as before, it is important to keep in mind that the big end is considered infinitely stiff.

5.2.4 Tension; Fixed Small End

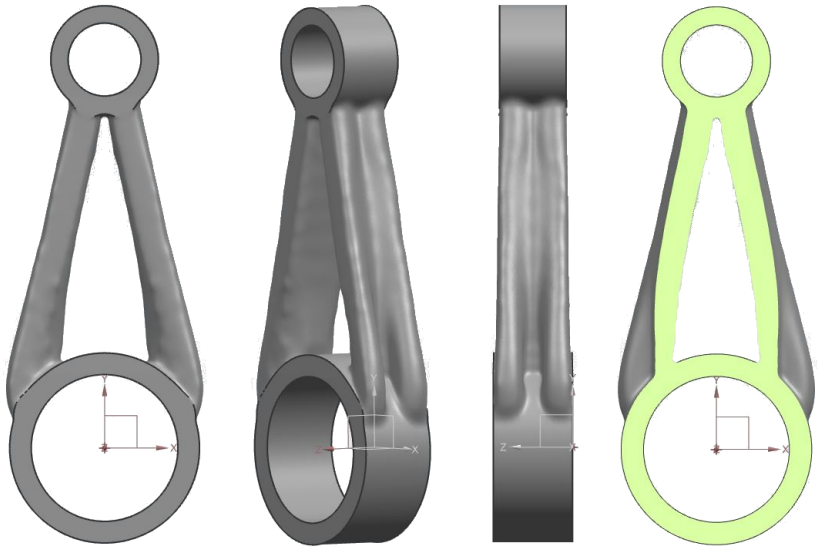

Figure 5.20: Best results from topology optimization, tension with fixed small end.

The best result of the last case is shown in Figure 5.20. In this case the bearing load was applied in the big end pointing in the negative Y-direction and the material spreading was, as in the other tension case, set to 30.

As for the previous tension case there are similarities to the compression case with the same constraints. The difference being the middle section of the beam that in the compression case compensated for the bearing force pointing upwards adding stresses to the top part of the big end. Here, these are not present and this middle part of the beam is therefore not present. Given that the sides were similar in both cases these were included in the final designs.

5.3 Final Results; Topology Optimization

In the end two designs were made based on the results of the four cases mentioned in the previous sections. These can be seen in Subsection 5.3.1 and Subsection 5.3.2, and will later be referred to as Design 2.0 and Design 2.1.

5.3.1 Design 2.0

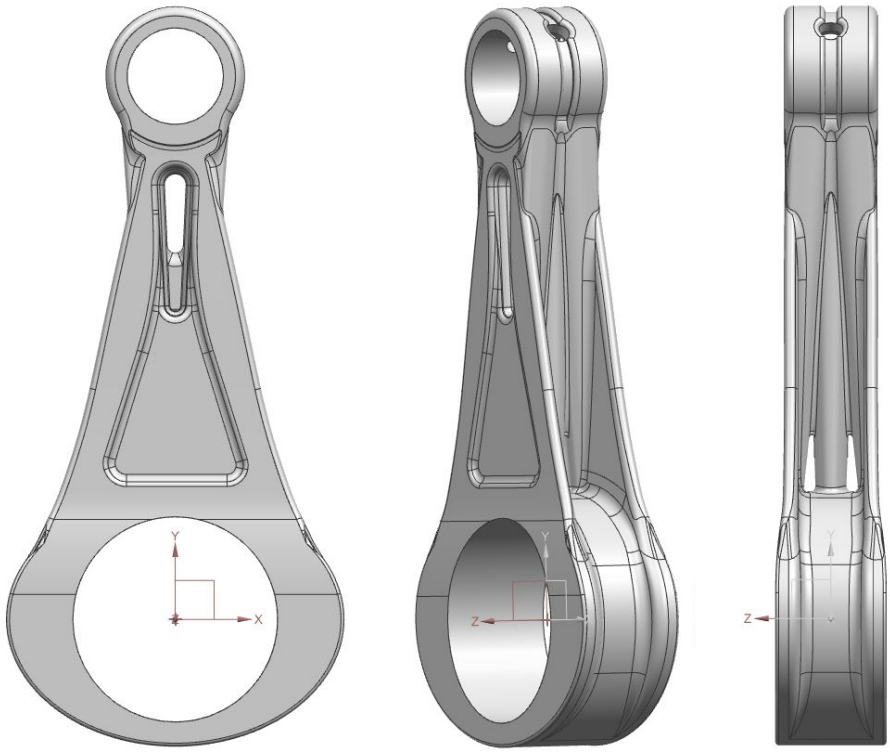

Figure 5.21: Design 2.0 from topology optimization results.

Design 2.0 looks like a very heavy rod with a beam section thickness of 15.2 mm, but it is in fact quite lightweight. This is due to its several hollow internal sections that are based on the design of the topology optimization results in Section 5.2.1 and Section 5.2.2. The cross sections of the beam going from bottom to top as well as from both sides can be viewed in the figures on the following pages.

The figures show the cross-sections to the left with the conrod seen from the front showing where it has been cut. The first four showing the cross-sections along the Y-axis, while the following four show the cross-sections in the X- and Z-directions respectively.

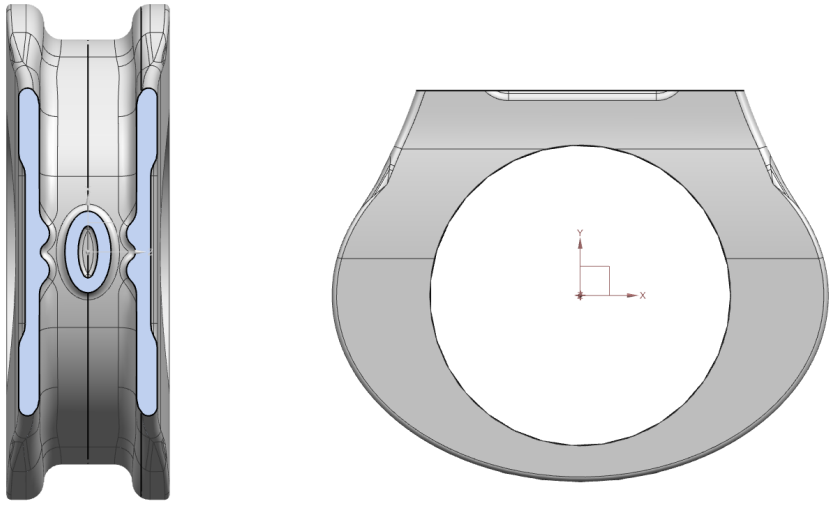

Figure 5.22: Cross-section of 2.0 beam; bottom beam section.

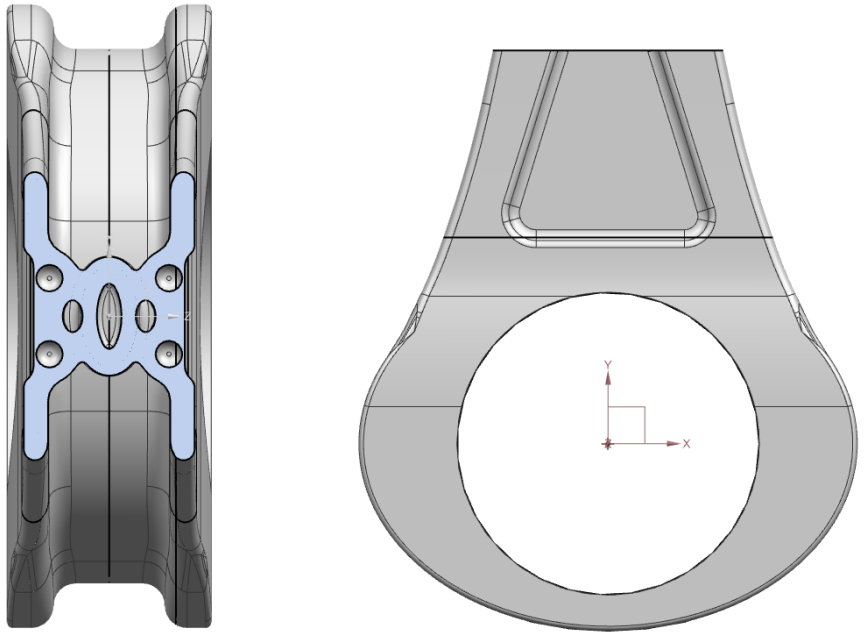

Figure 5.23: Cross-section of 2.0 beam; lower middle beam section.

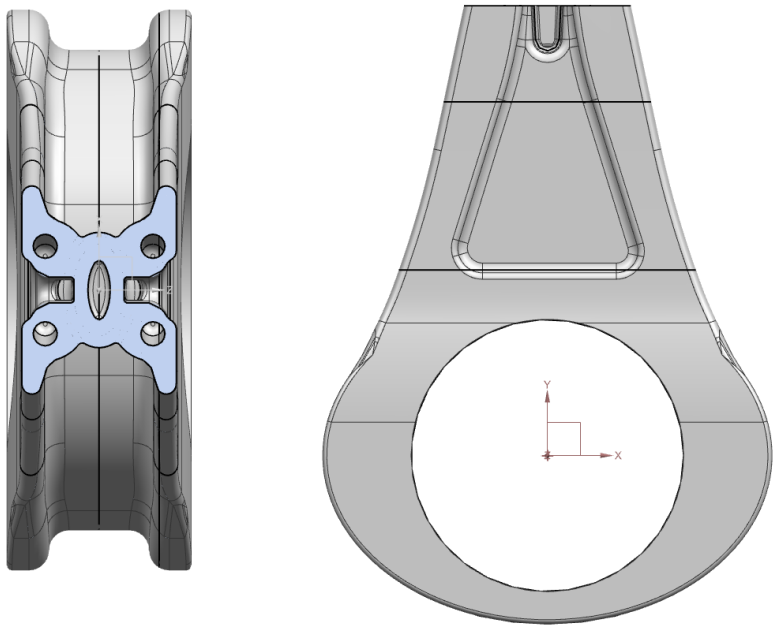

Figure 5.24: Cross-section of 2.0 beam; upper middle beam section.

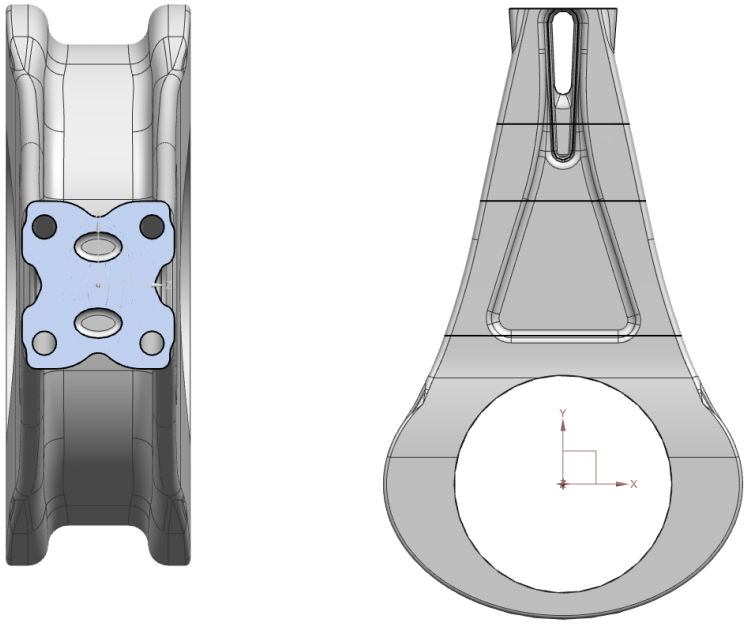

Figure 5.25: Cross-section of 2.0 beam; top beam section.

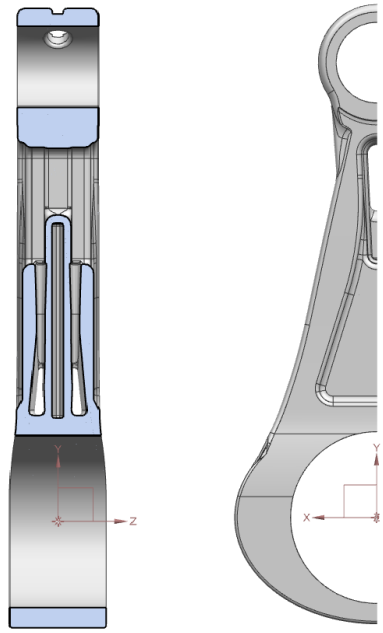

Figure 5.26: Cross-sections of 2.0 beam about X-axis; Center cut.

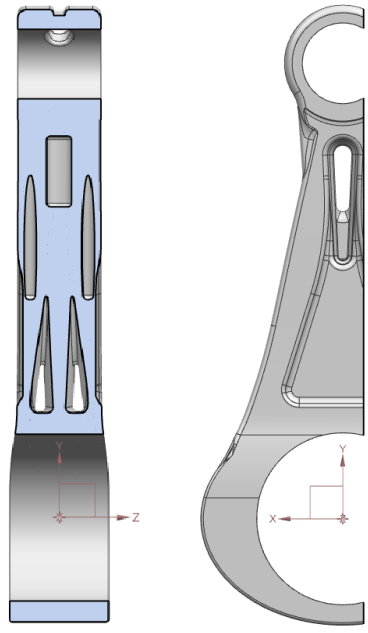

Figure 5.27: Cross-sections of 2.0 beam about X-axis; Outer cut.

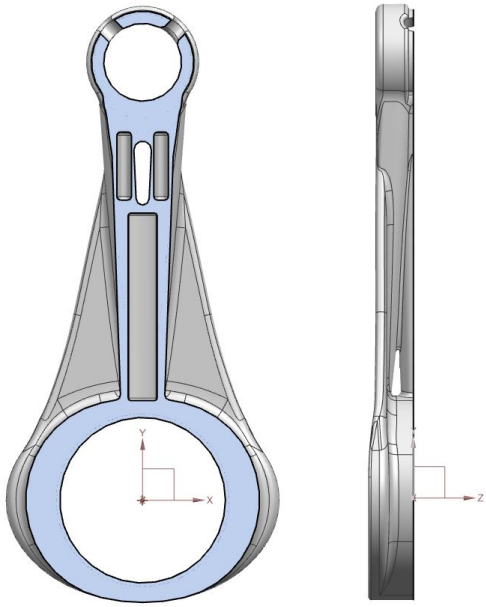

Figure 5.28: Cross-sections of 2.0 beam about Z-axis; Center cut.

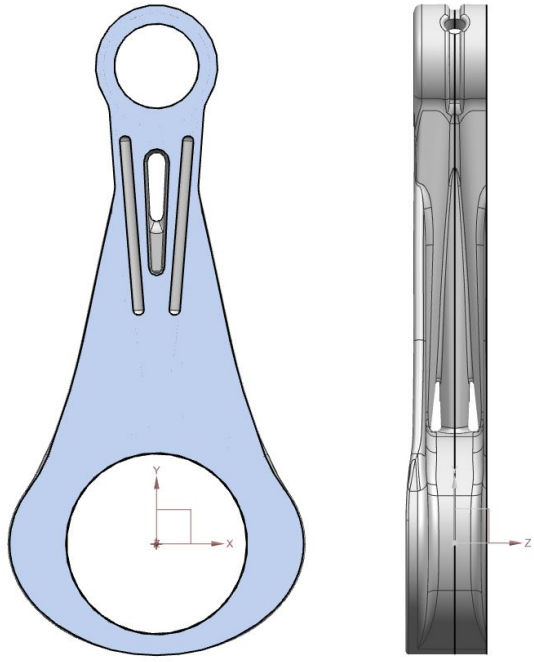

Figure 5.29: Cross-sections of 2.0 beam about Z-axis; Outer cut.

5.3.2 Design 2.1

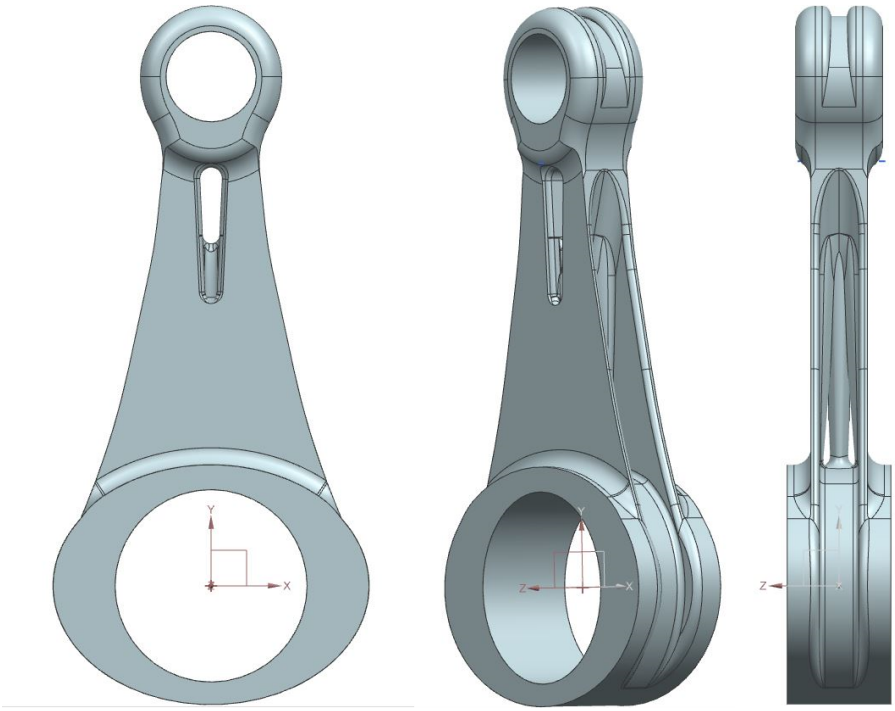

Figure 5.30: Design 2.1 from topology optimization results.

As for Design 2.0, Design 2.1 contains internally hollow sections based on the designs from the topology optimization of Section 5.2.1 and Section 5.2.2. The beam section here is 10 mm thick.

The figures show cross-sections in the same order as in Section 5.3.1, with the cross-section to the left of the figure and the conrod seen from the side or the front, showing where it has been cut.

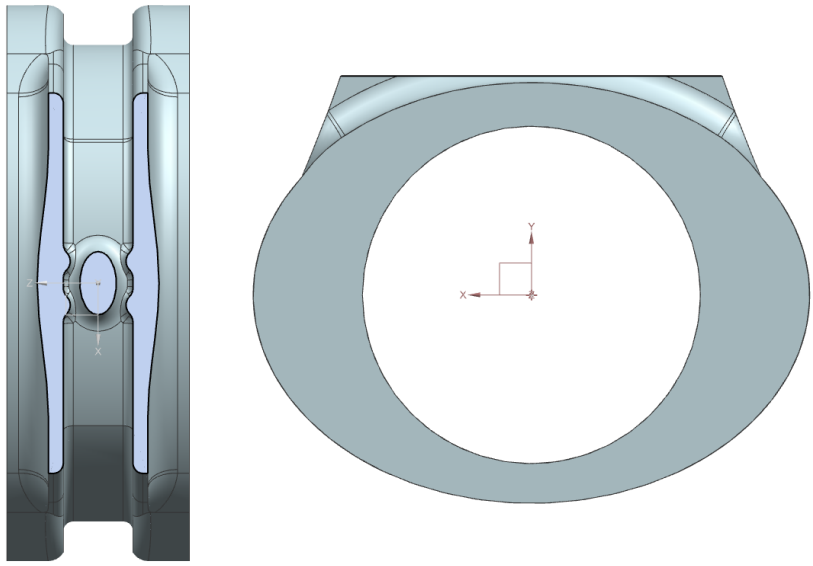

Figure 5.31: Cross-section of 2.1 beam; bottom beam section.

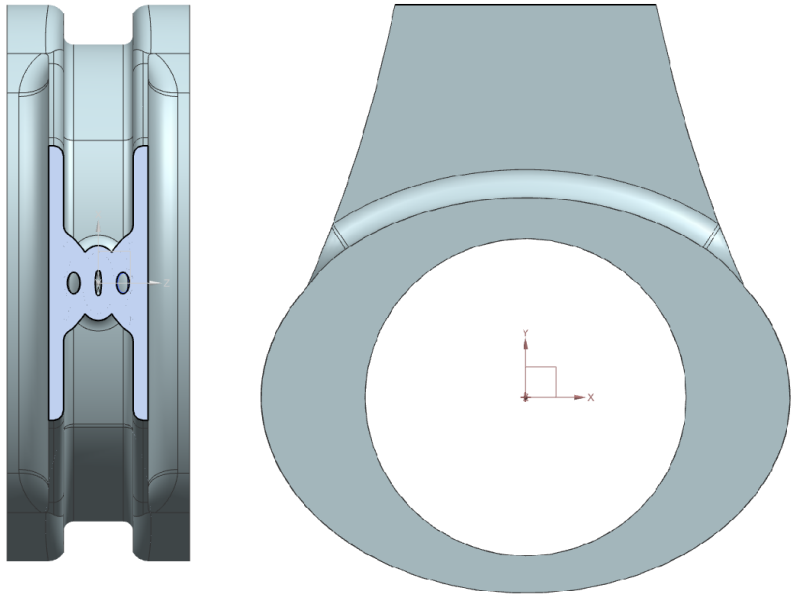

Figure 5.32: Cross-section of 2.1 beam; lower middle beam section.

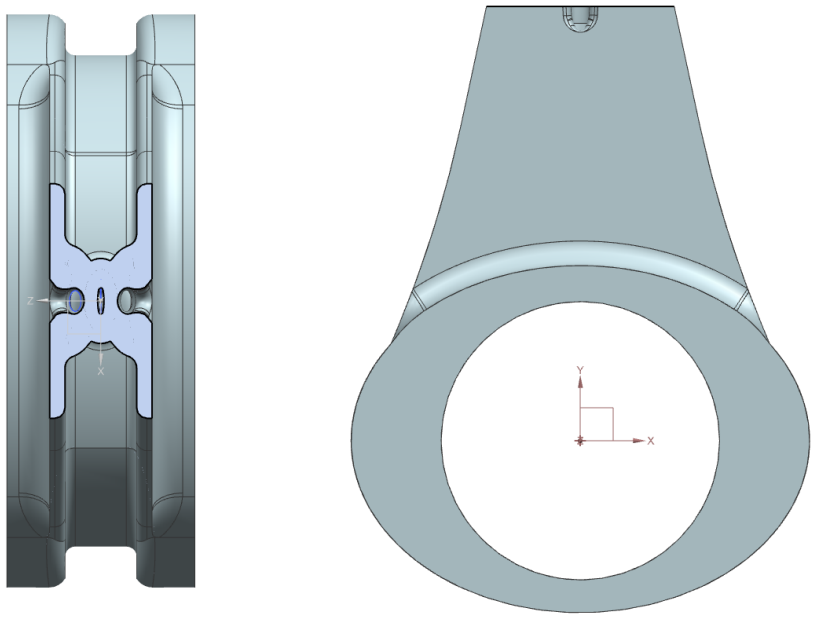

Figure 5.33: Cross-section of 2.1 beam; upper middle beam section.

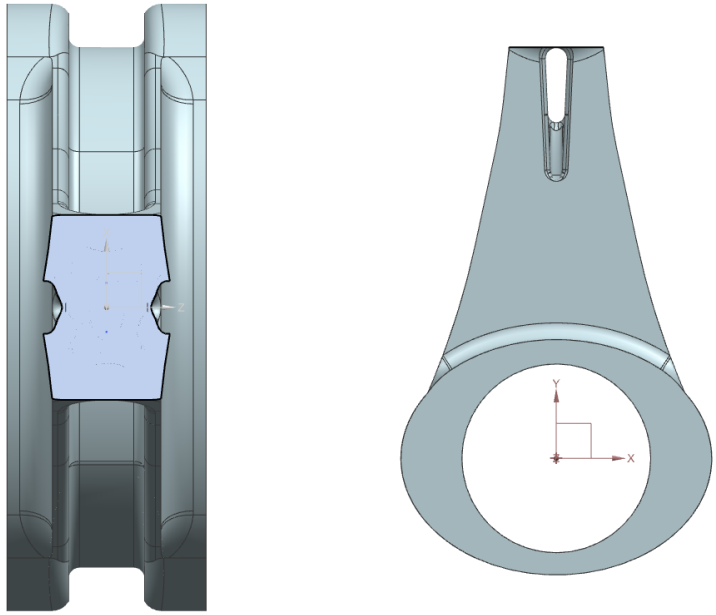

Figure 5.34: Cross-section of 2.1 beam; top beam section.

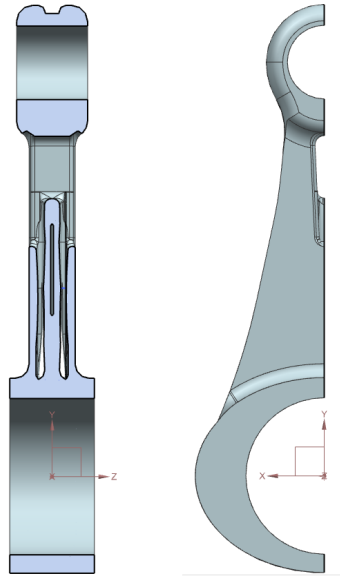

Figure 5.35: Cross-sections of 2.1 beam about X-axis; Center cut.

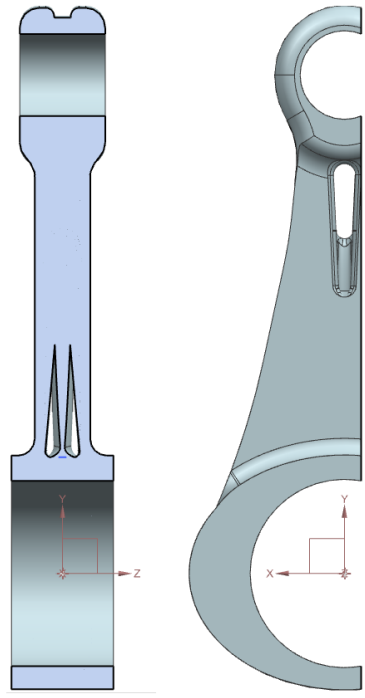

Figure 5.36: Cross-sections of 2.1 beam about X-axis; Outer cut.

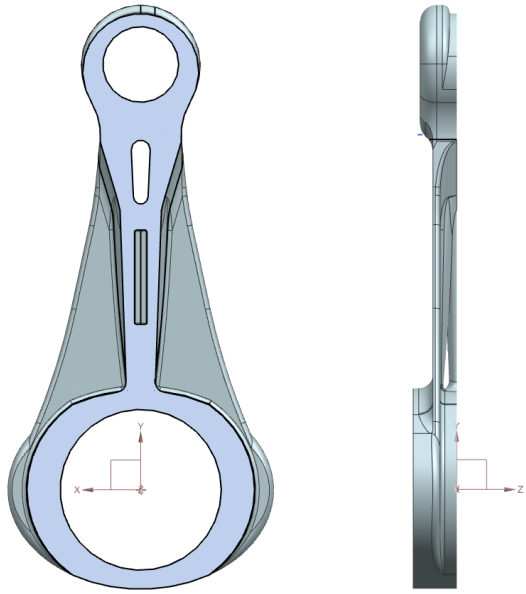

Figure 5.37: Cross-sections of 2.1 beam about Z-axis; Center cut.

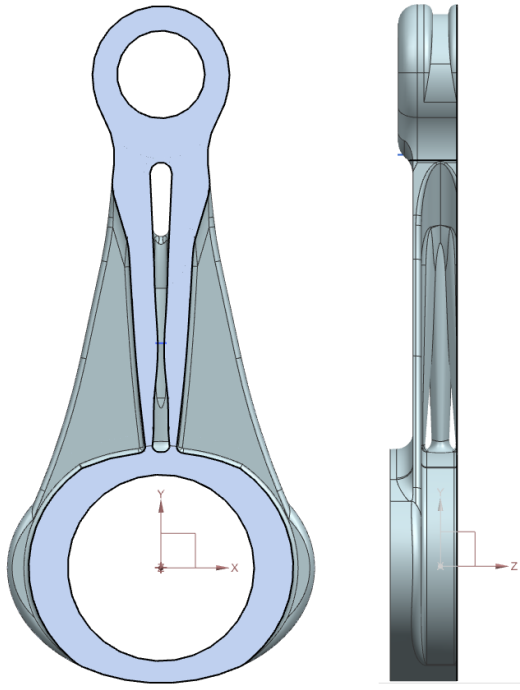

Figure 5.38: Cross-sections of 2.1 beam about Z-axis; Outer cut.

5.3.3 Mechanical properties Design 2.0 and Design 2.1

The mass properties of Design 2.0 can be seen in Figure 5.39 below. As opposed to the traditional approach conrod, the reference coordinate system is the one described in the beginning of Section 5.2. The material selected is also here Ti6Al4V.

```
Measurement Mass Properties

Displayed Mass Property Values
Volume                          = 27617.933979472 mm³
Area                            = 17741.198072447 mm²
Mass                            =    0.122347448 kg
Weight                          =    1.199818596 N
Radius of Gyration              =   37.514092024 mm
Center of Mass                  =    0.002649733,   28.046305764,   -0.000221856 mm
```

Figure 5.39: Mass properties of Design 2.0.

Figure 5.40 shows the mass properties of Design 2.1. The reference coordinate system is the same as for Design 2.0 and the material selected is also Ti6Al4V.

```
Measurement Mass Properties

Displayed Mass Property Values
Volume                          = 28233.400151672 mm³
Area                            = 15734.675456904 mm²
Mass                            =    0.125073963 kg
Weight                          =    1.226556576 N
Radius of Gyration              =   38.945237407 mm
Center of Mass                  =   -0.000532107,   27.406187265,   -0.000009162 mm
```

Figure 5.40: Mass properties of Design 2.1.

5.3.4 Meshing Design 2.0 and Design 2.1

CTETRA(10) was chosen as the mesh type for both Design 2.0 and 2.1 with an element size of 1.6 mm and 1.5 mm respectively. In addition to a small element size the SCBSV were increased to 60% and 75.2%.

For Design 2.0 the failed element fraction was about 0.6% without any significant warning elements. The failed element fraction for Design 2.1 was 0.3%, and as for Design 2.0 it didn't have any significant warning elements.

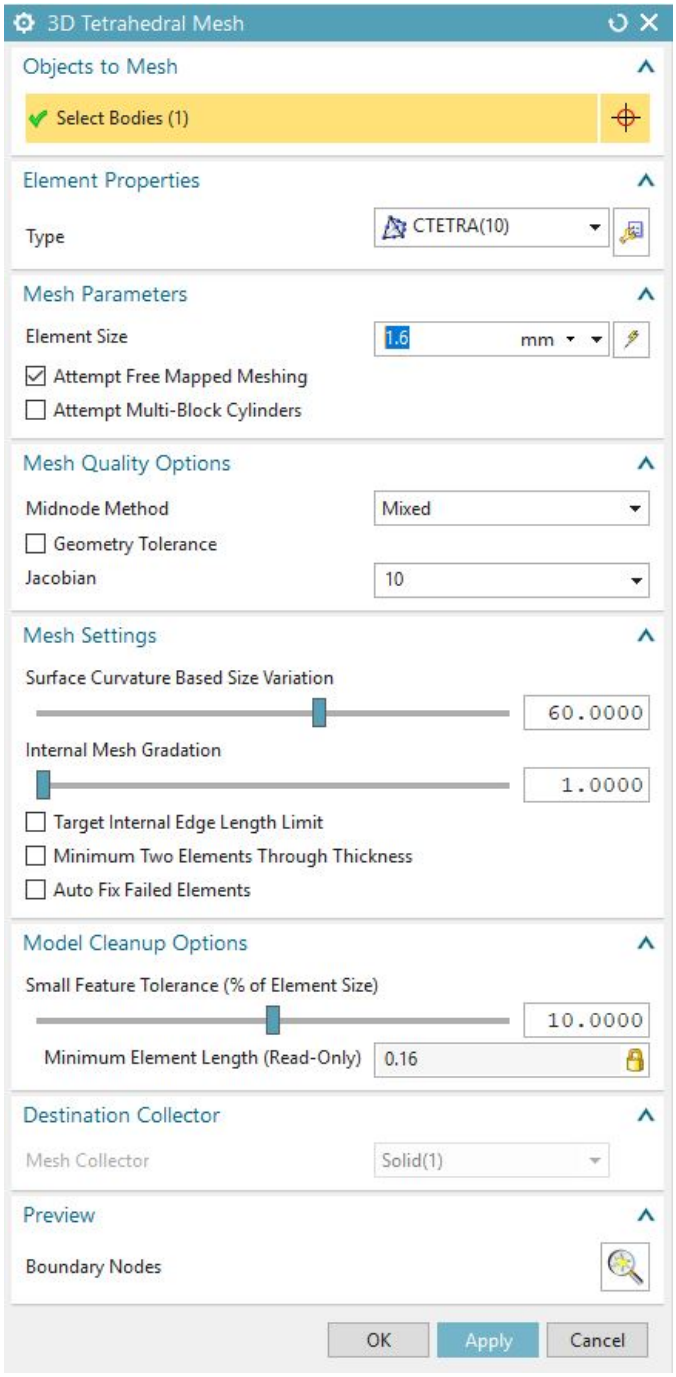

Figure 5.41: Mesh features; Design 2.0.

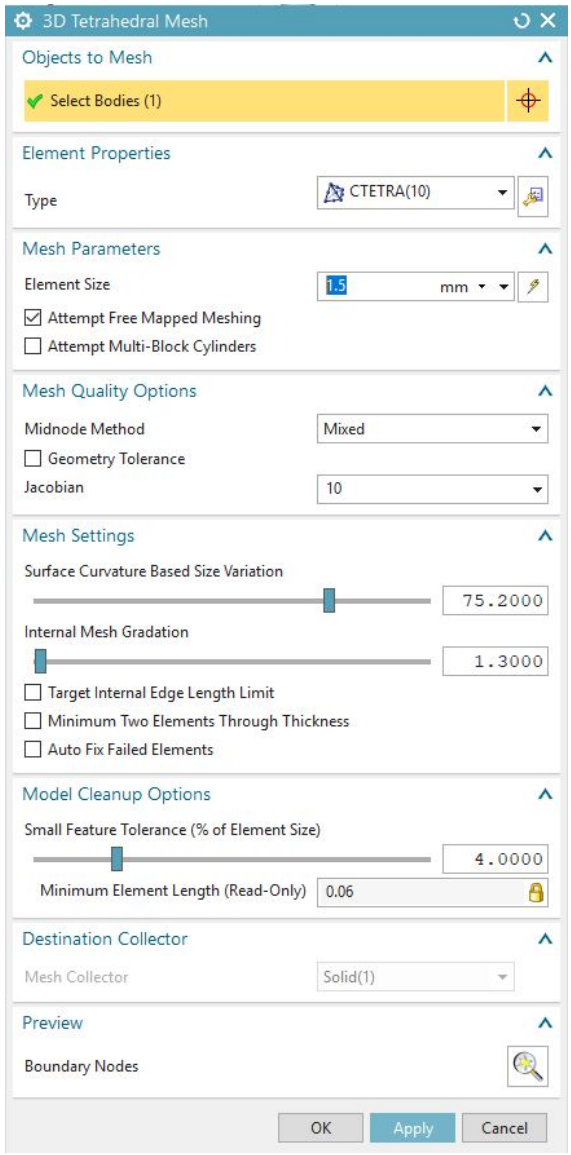

Figure 5.42: Mesh features; Design 2.1.

5.3.5 Static Analysis in NX; Design 2.0 and 2.1

Both Design 2.0 and 2.1 were analyzed statically in NX before approving them for further analysis. The changes that were made focused primarily on removing critical stress concentrations by smoothing out surfaces and edges. The final static analyses can be seen in Figure 5.43 and Figure 5.44. The maximum stresses are indicated in the annotation boxes in the figures and are 834.7 MPa and 822.4 MPa for Figures 5.43 and 5.44 respectively.

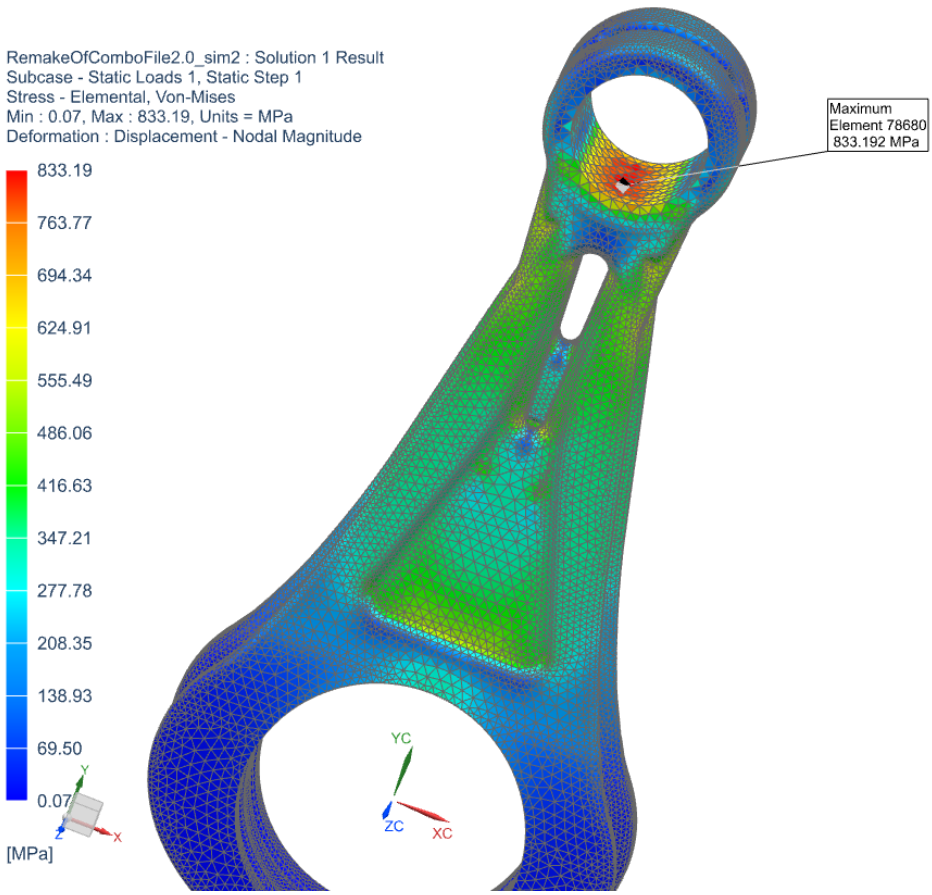

Figure 5.43: Static analysis of Design 2.0

The maximum stresses in Design 2.0 were located inside the small end, and will in reality, as for the Traditional Approach conrod, be significantly lower once the piston pin is inserted and the forces are applied more precisely in FEDEM. The rest of the connecting rod has stresses well below 650 MPa, and with a maximum deformation of 308 μm, the result was considered good enough to continue in FEDEM.

For Design 2.1 the maximum stresses are located within the hollow section at an edge blend. Exept for these stress concentration the rest of the conrod experiences stresses no greater than 750 MPa. Considering that the stresses would decrease when applying the load more precisely in FEDEM, and with a maximum deformation of 293 μm, even lower than for Design 2.0, these results were considered good enough to continue as well.

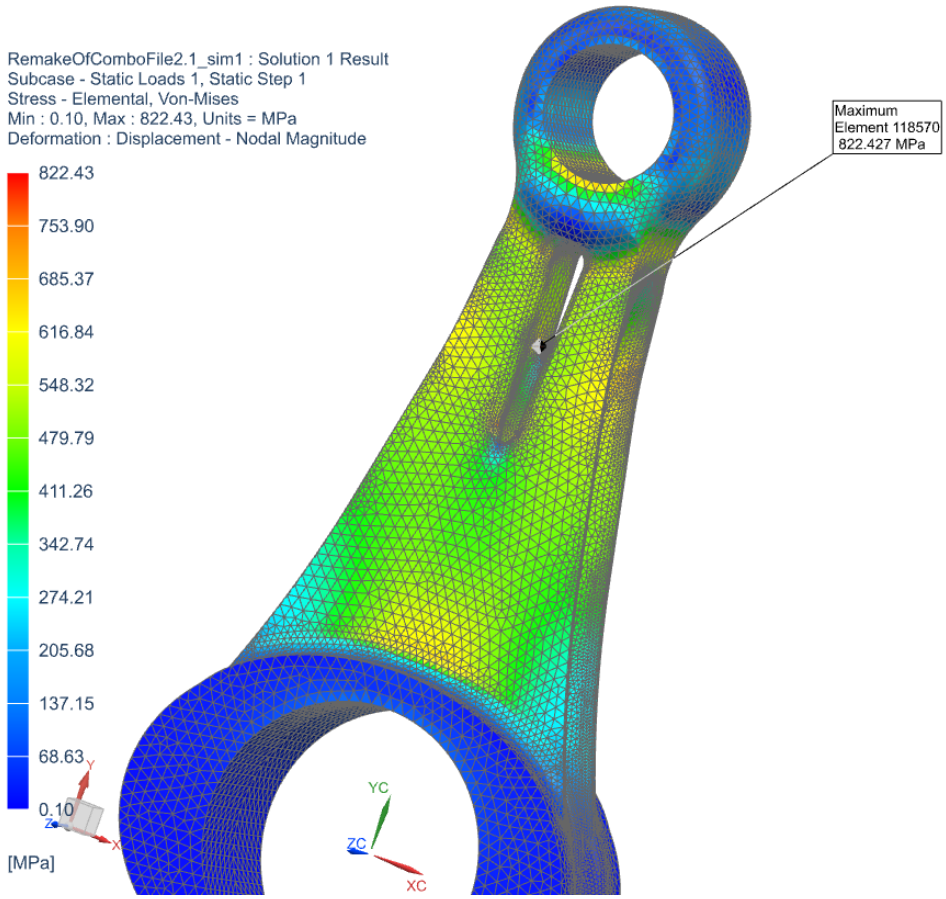

Figure 5.44: Static analysis of Design 2.1

5.3.6 Stiffness Analysis

A stiffness analysis was performed on both Design 2.0 and Design 2.1 described in Subsections 5.3.1 and 5.3.2. For these analyses 15 cross-sections for Design 2.0 and 14 cross-sections for Design 2.1 of the conrod beam were looked at. The results can be seen in Figure 5.45 and Figure 5.46.

As can be seen from the figures, the moment of inertia decreases about both axes towards the small end. This is expected given that the total area gets smaller closer to the small end.

For Design 2.0 the area of the beam section moves closer and closer towards a cross-section with equal stiffness about both axes going from big end to small end, as can be seen clearly from the graph as well as the values in the table below. The minimum moment of inertia for Design 2.0 is 2570 mm^4 about the X-axis and 3210 mm^4 about the Z-axis.

When it comes to Design 2.1 the beam area has an almost constant stiffness about the

X-axis, with the Z-axis stiffness varying quite a bit more, moving from big end to small end. The minimum moment of inertia for Design 2.1 is 1100 mm^4 about the X-axis and 2790 mm^4 about the Z-axis.

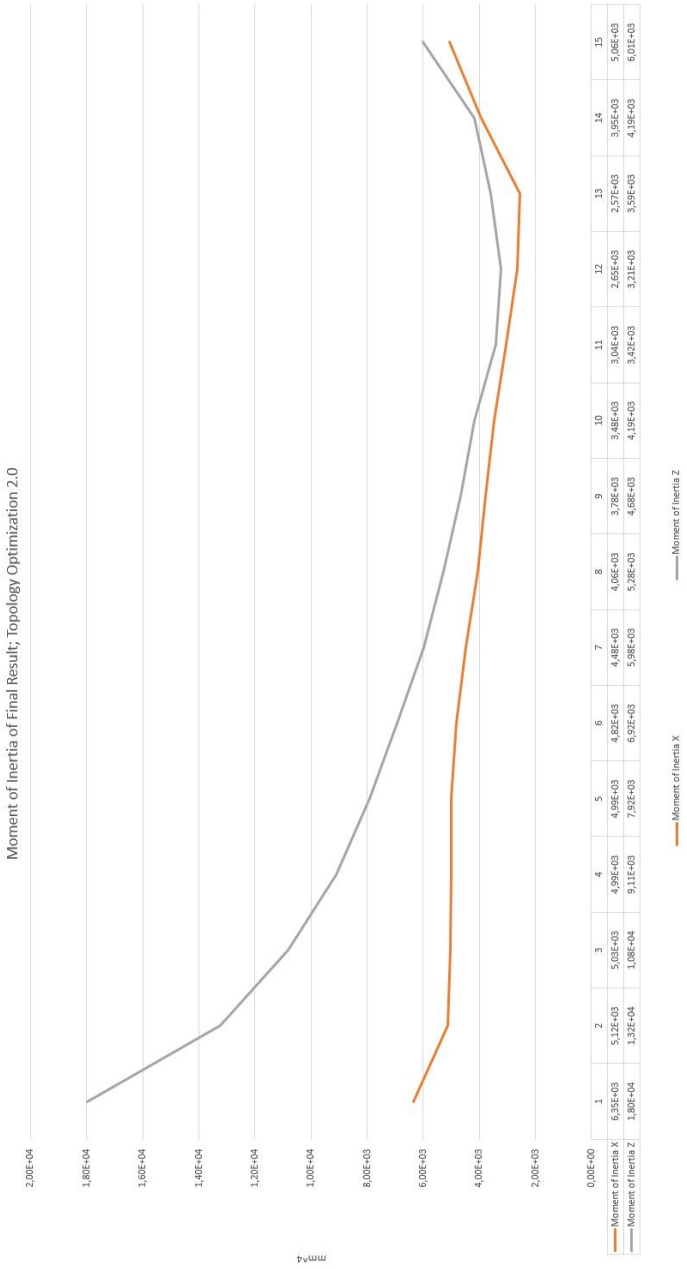

Figure 5.45: Moment of Inertia of beam section, Topology Optimization 2.0.

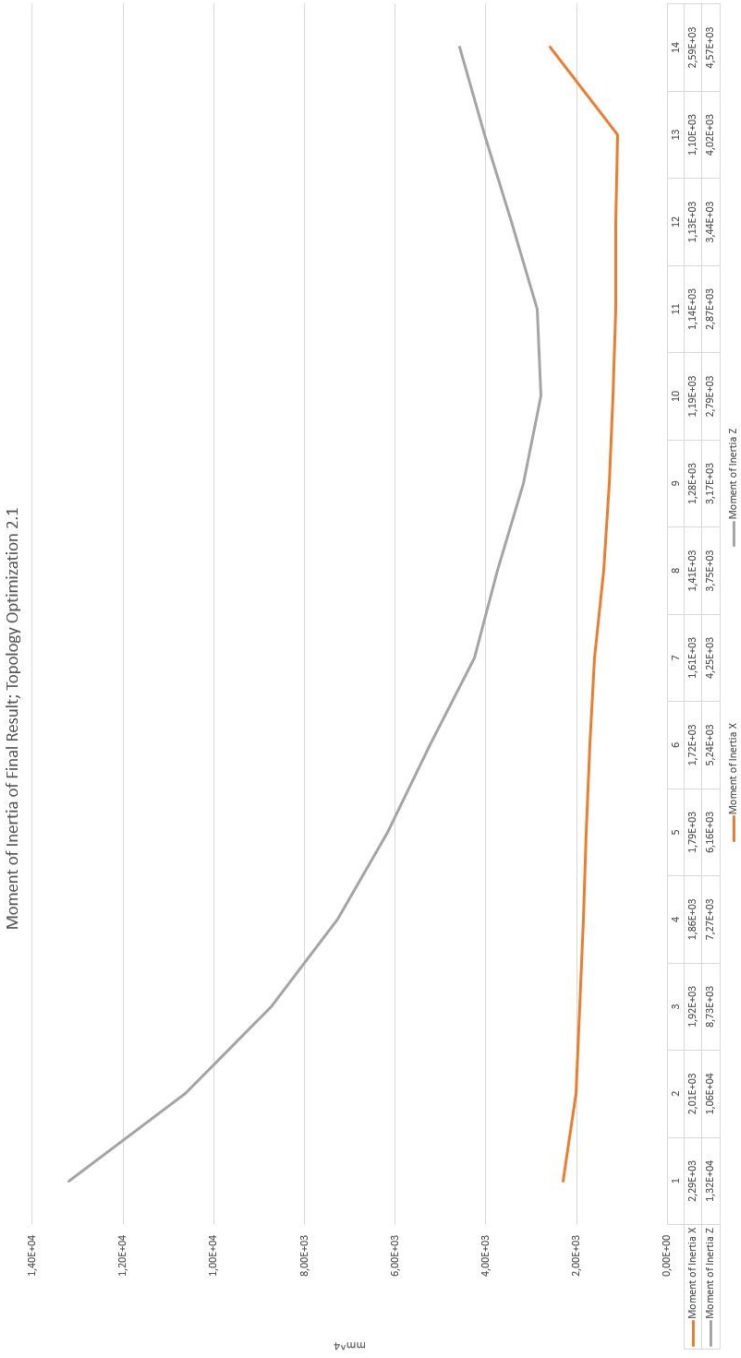

	1	2	3	4	5	6	7	8	9	10	11	12	13	14
Moment of Inertia X	2,29E+03	2,01E+03	1,92E+03	1,86E+03	1,79E+03	1,72E+03	1,61E+03	1,41E+03	1,28E+03	1,19E+03	1,14E+03	1,13E+03	1,10E+03	2,59E+03
Moment of Inertia Z	1,32E+04	1,06E+04	8,73E+03	7,27E+03	6,16E+03	5,24E+03	4,25E+03	3,75E+03	3,17E+03	2,79E+03	2,87E+03	3,44E+03	4,02E+03	4,57E+03

Figure 5.46: Moment of Inertia of beam section, Topology Optimization 2.1.

5.3.7 FEDEM Analysis of Final Results; Topology Optimization

As done with the traditional approach conrod both Design 2.0 and Design 2.1 were inserted into the FVTB to check their performance in a dynamic analysis. Design 2.0 and Design 2.1 would also be put up against the MXRR conrod, with both conrods inserted in the same motor block with the same components as the traditional approach conrod.

A bob weight calculation using the mass properties given in Subsection 5.3.3, was also necessary for Design 2.0 and Design 2.1 to continue the analysis in FEDEM. These calculations can be seen in Figures 5.47 and 5.48. Just as for the traditional approach conrod the bob weights can be seen in Figures 5.49 and 5.56 as small green coordinate systems at the bottom of the crankshafts.

	TopOptRod2.0	
MXRR	big end	small end
Bearing	39	
RodWeight	84,22	
Oil etc	5	
Piston Pin		27
Piston		158
RodWeight		38,13
Factor		0,28
BobWeight	190,6964	
Balance	103,2	
per node	51,6	

TopOptRod2.0 weight	122,35
% small end	31
% big end	69

Figure 5.47: Calculation of Bob weights for Design 2.0.

	TopOptRod2.1	
MXRR	big end	small end
Bearing	39	
RodWeight	86,98	
Oil etc	5	
Piston Pin		27
Piston		158
RodWeight		38,09
Factor		0,28
BobWeight	193,4452	
Balance	104,7	
per node	52,4	

TopOptRod2.1 weight	125,07
% small end	30
% big end	70

Figure 5.48: Calculation of Bob weights for Design 2.1.

FEDEM Analysis of Design 2.0

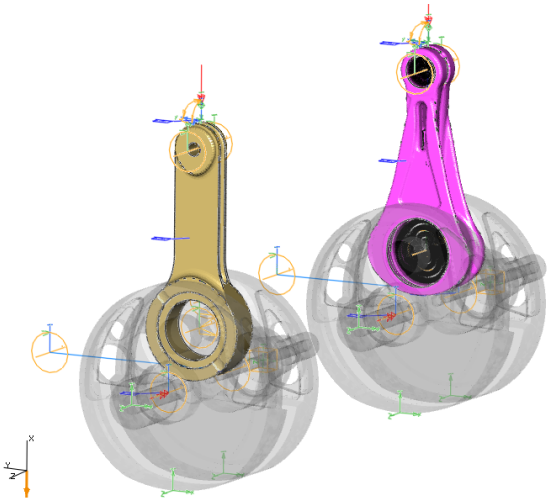

Figure 5.49: Conrod 2.0 in FVTB next to MXRR conrod.

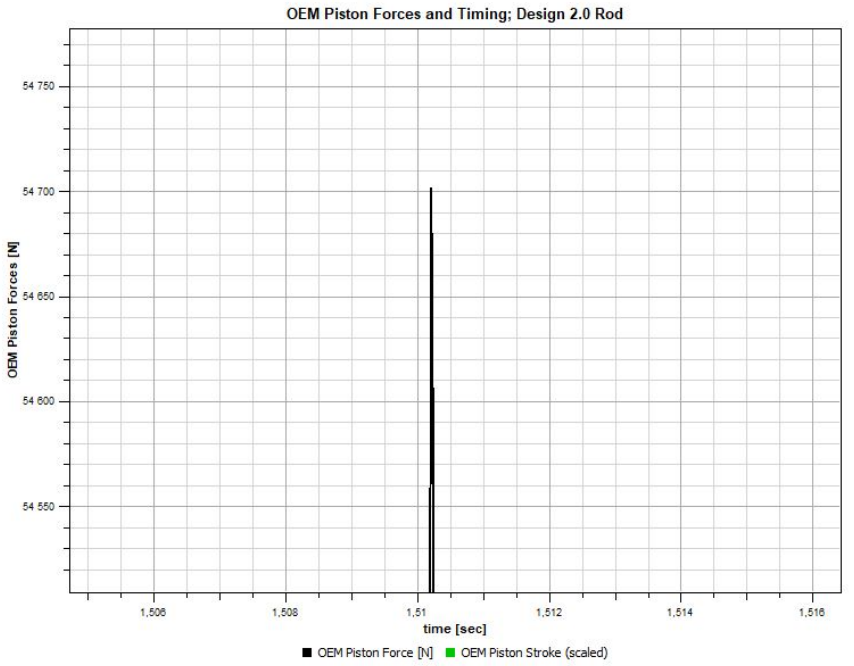

Figure 5.50: Maximum piston force applied to conrod 2.0

Figure 5.50 shows the timing and value of the maximum piston force applied to Design 2.0. The force is referred to as an OEM piston force since the motor is an OEM motor. As can be seen in the figure the value of the force is about 54.7 kN and occurs around 1.51025 seconds. The stresses recovered when testing the maximum Von Mises stress are recovered around this force peak.

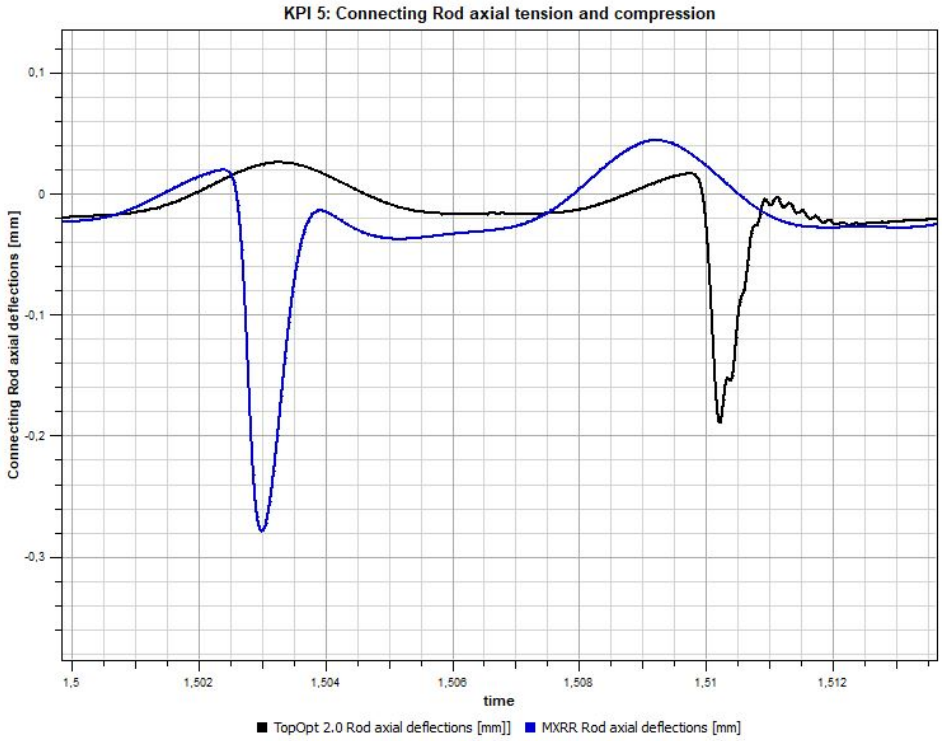

Figure 5.51: Maximum axial deformation for Design 2.0 next to maximum MXRR conrod deflection.

Maximum axial compression and tension can be seen in Figure 5.51. The value of the compression is at around 190 μm almost 100 μm less than the deflection on the MXRR conrod. The strain of the conrod is also observably lower for Design 2.0.

The maximum crank speed is illustrated in Figure 5.52, and it's the black line that indicates the value of the Design 2.0 conrod. The value can be estimated to be around 14900 RPM, from the graph, about 350 RPM higher that for the MXRR conrod.

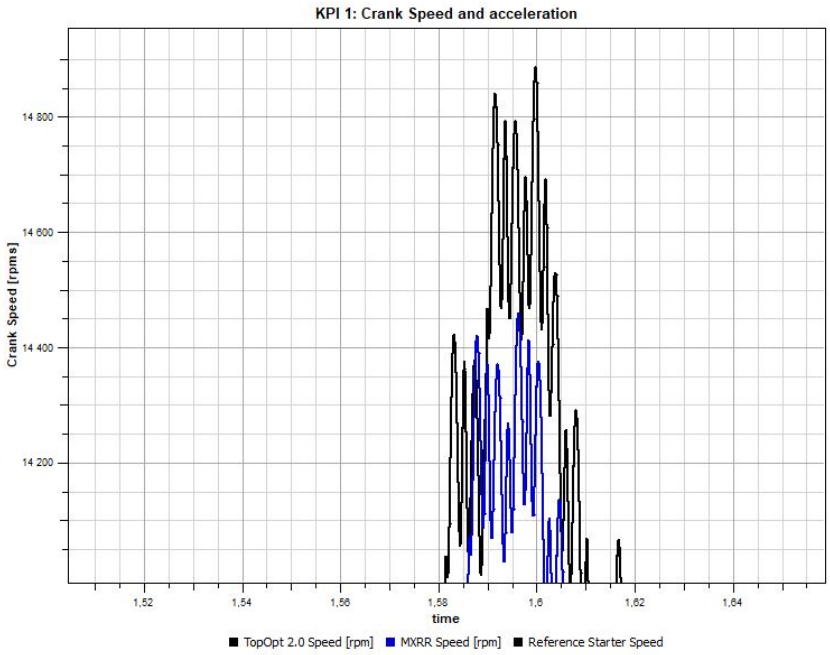

Figure 5.52: Maximum crank speed achieved for Design 2.0.

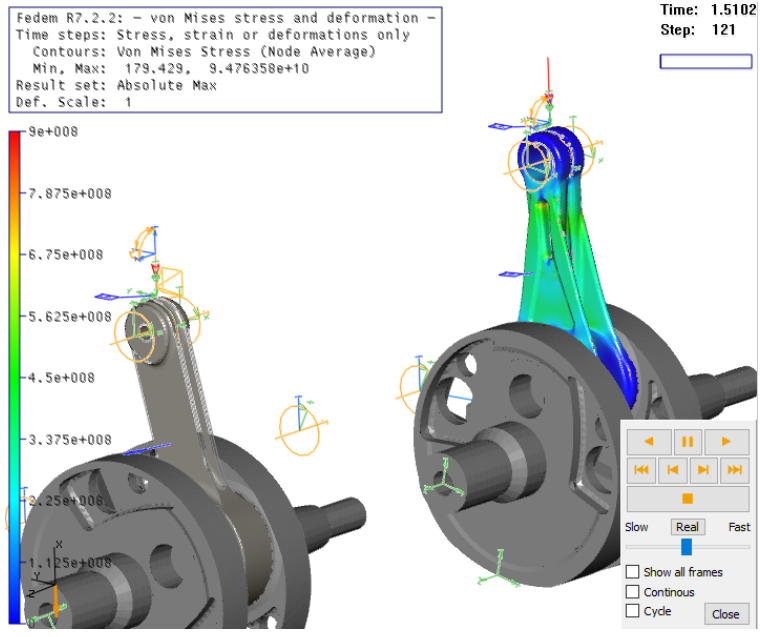

Figure 5.53: Von Mises stress overview in FEDEM; Design 2.0.

When looking at the stresses occurring in Design 2.0 during a cycle most of the beam section has stresses around 500-600 MPa; Seen in Figure 5.53. After having inspected the beam closer small stress concentrations with values of over 900 MPa were discovered, as can be seen in Figures 5.54 and 5.55. These stress concentrations have been marked with black circles.

The three elements circled in the two figures are the only elements visible that are still glowing red when changing the scale to indicate a maximum above the 900 MPa used in the figures. Their mirrored elements about the axes of symmetry show stresses between 300 and 600 MPa, as does neighbouring elements.

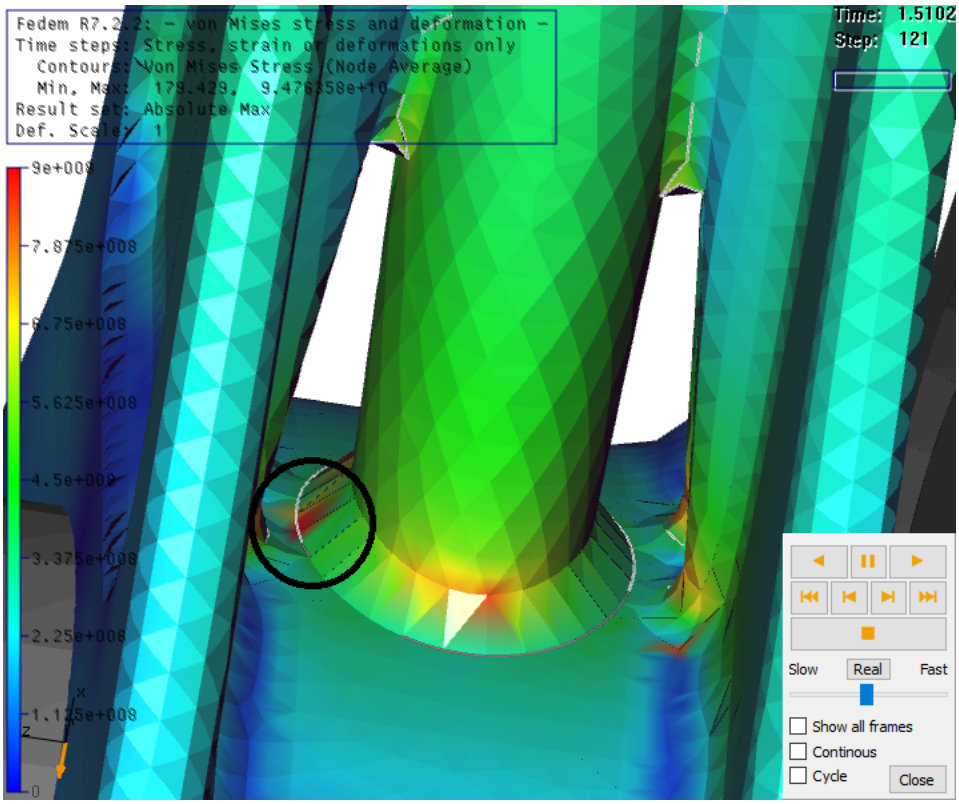

Figure 5.54: Stress concentrations in lower beam section; Design 2.0.

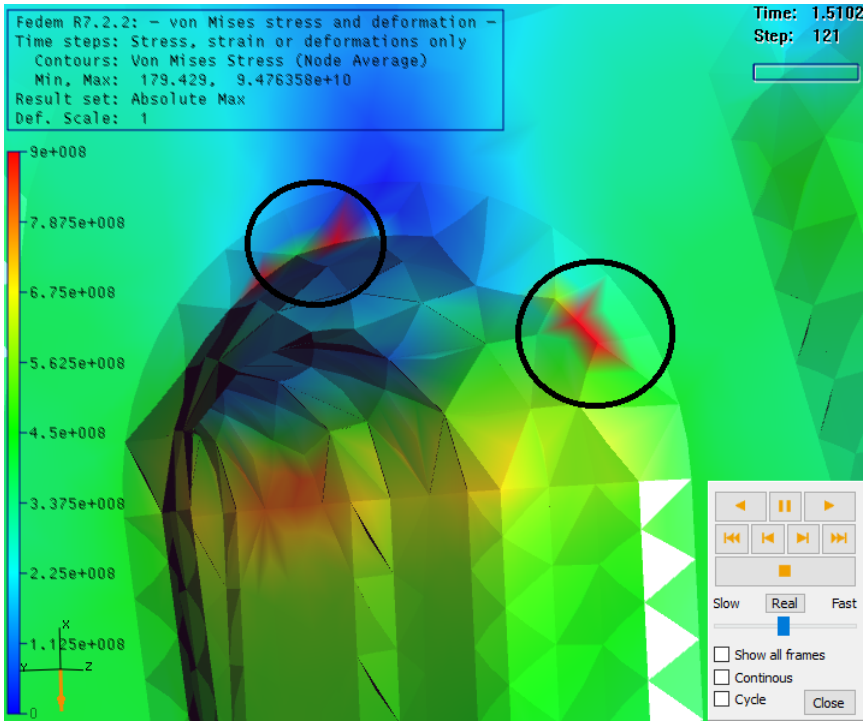

Figure 5.55: Stress concentrations in upper beam section; Design 2.0.

FEDEM Analysis of Design 2.1

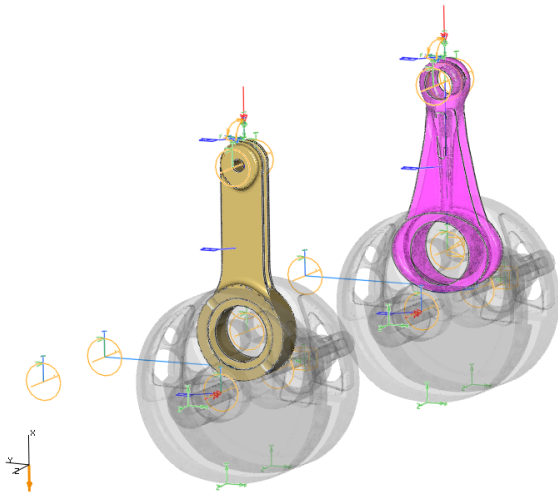

Figure 5.56: Conrod 2.1 in FVTB next to MXRR conrod.

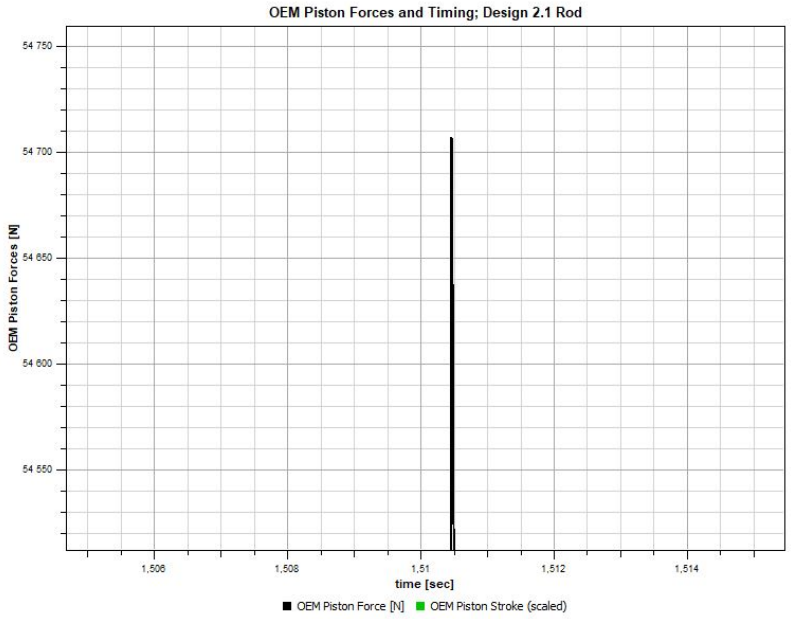

Figure 5.57: Maximum piston force applied to conrod 2.1

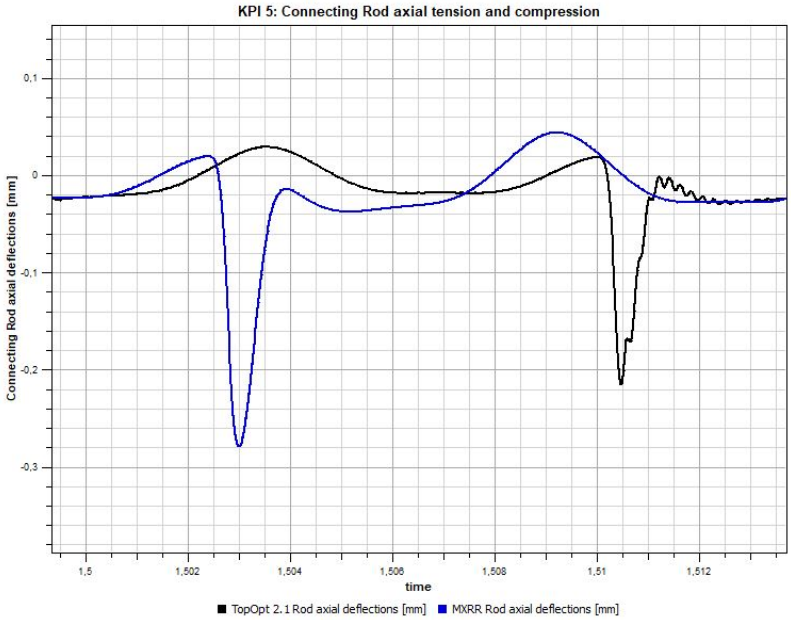

Figure 5.58: Maximum axial deformation for Design 2.1 next to maximum MXRR conrod deflection.

Figure 5.57 shows the timing and value of the maximum piston force applied to Design 2.1. The maximum of 54.7 kN occurs at about 1.5105 seconds, and the stresses recovered at this point will be shown later in this subsection.

The maximum axial compression for Design 2.1 can be read from Figure 5.58 to be approximately 220 μm, about 60 μm less than for the MXRR conrod. As for Design 2.0 the strain of Design 2.1 is notably lower than for the MXRR conrod.

In Figure 5.59 below, the maximum crank speed achieved with Design 2.1 is illustrated. Again there is a significant difference in maximum RPM achieved between the MXRR conrod and the new design, as much as 500 RPM's separates the output from the two connecting rods.

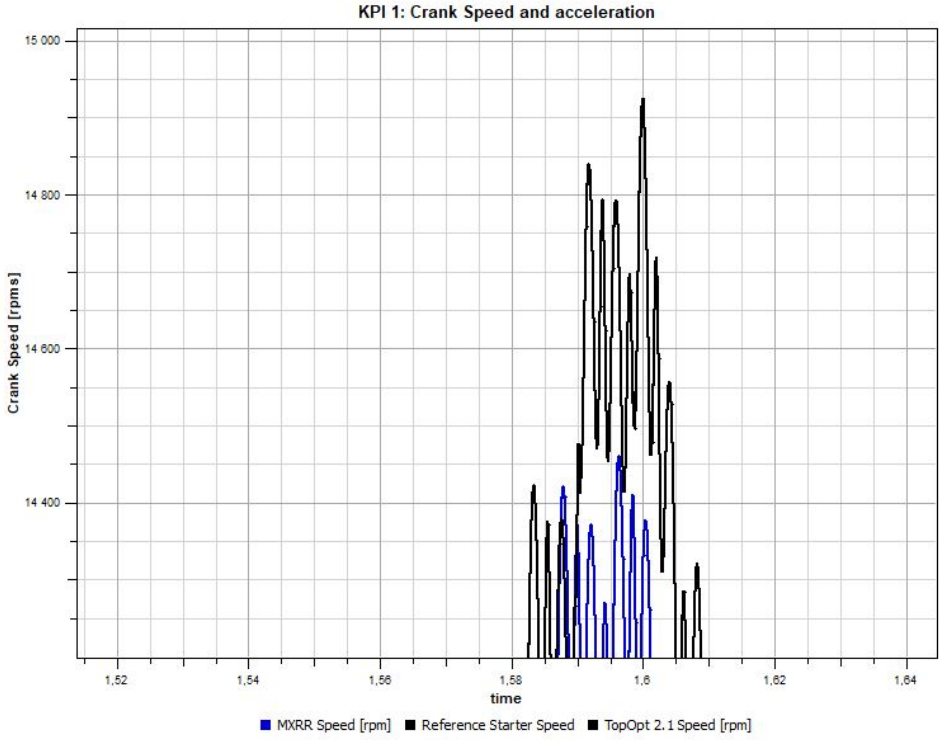

Figure 5.59: Maximum crank speed achieved for Design 2.1.

Stress levels on Design 2.1 are mostly below 700 MPa with a few exceptions, as can be seen in Figures 5.60, 5.62 and 5.61. Stresses are around 800 MPa around the connecting areas between big end and the beam, as well as where the beam meets the small end. These stresses are symmetrical and identical on both sides of the axis of symmetry.

The only visible elements of the conrod with stress levels above 900 MPa are the two elements inside the red circle on Figure 5.62. By changing the scale to have a maximum of 8.0 GPa the entirety of the conrod turns blue, except for these two elements that remain glowing red.

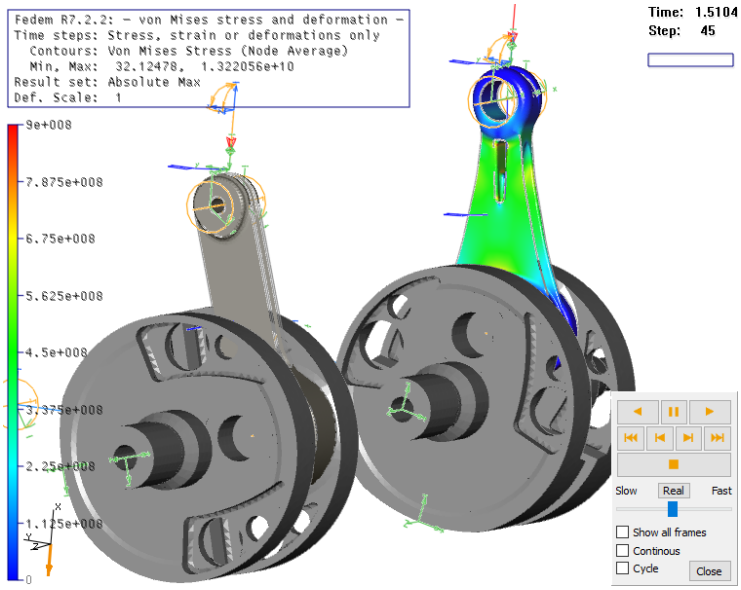

Figure 5.60: Von Mises stress overview in FEDEM; Design 2.1.

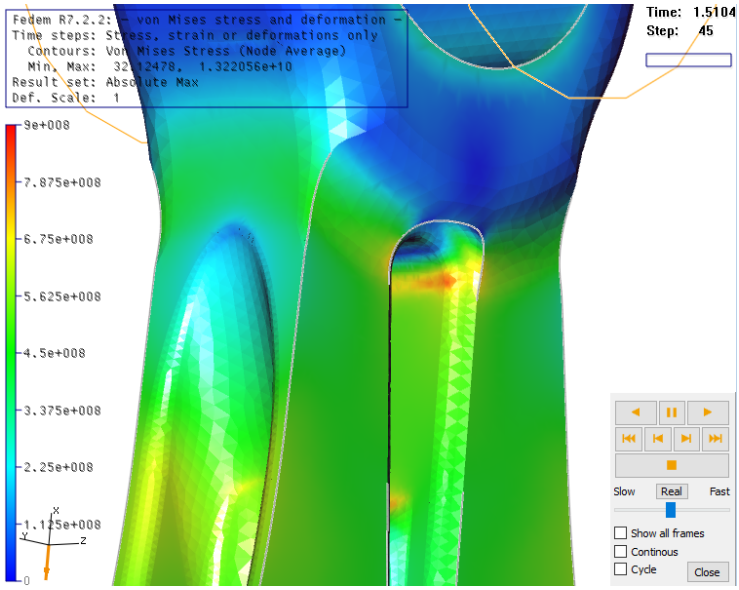

Figure 5.61: Stress concentrations in upper beam section; Design 2.1.

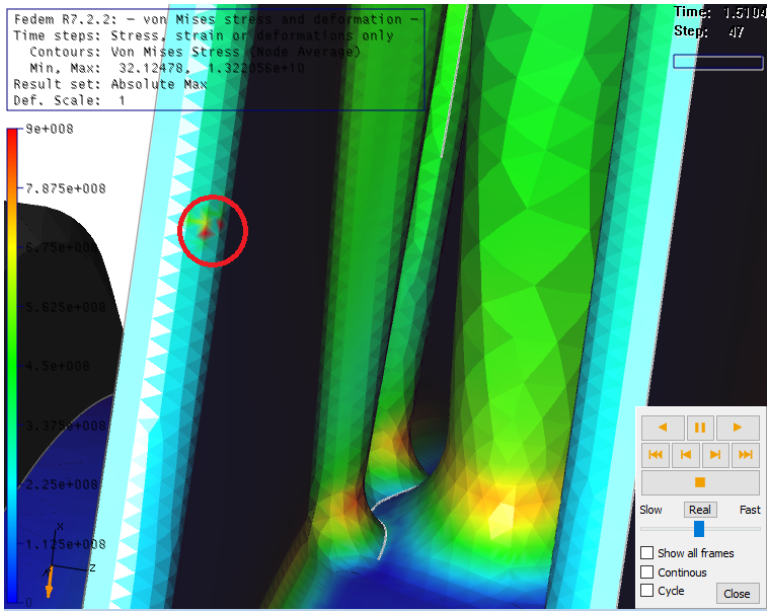

Figure 5.62: Stress concentrations in lower beam section; Design 2.1.

Chapter 6

Discussion

The discussion of the results will follow in this chapter. The figure below, Figure 6.1, sums up the results from chapter 5 and will be used as a reference to this chapter.

	CRF250R	CRF250R	CRF250R	CRF250R
Connecting rod	Traditional approach	Design 2.0	Design 2.1	OEM
Mass	123.02 g	122.35 g	125.07 g	129.56 g
Small end/Big end mass ratio	32/68	31/69	30/70	26/74
Bob weights	190.85 g	190.70 g	193.45 g	200.88 g
Max. Von Mises stress	882.4 MPa	Approx. 800 MPa	Approx. 800 MPa	-
Max. compression	160 µm	190 µm	220 µm	280 µm
Max. RPM achieved	Approx. 14,880	Approx. 14,880	Approx. 14,925	Approx. 14,450
Material	Ti6Al4V	Ti6Al4V	Ti6Al4V	MXRR Titanium
Min. moment of inertia; X-axis	1830 mm^4	2570 mm^4	1100 mm^4	852.7 mm^4
Min. moment of inertia; Z-axis	3200 mm^4	3210 mm^4	2790 mm^4	3590 mm^4

Figure 6.1: Summary of results.

6.1 Creating Design 2.0 and 2.1

The initial idea when utilizing topology optimization was to mesh the results directly and perform simulations on these before joining the best features in one part. But as mentioned in section 4.2, this proved more difficult than expected.

Design 2.0 was created first, and Design 2.1 was created as a ”slimmer” copy of it by scaling down the different parts of the beam section. A variety of sweep and extrude commands along with edge blend were applied to best imitate the organic structures. Having a

5.2 mm narrower beam section than its predecessor, Design 2.1 was limited to only a few internal hollow features to be able to keep its stiffness.

The center column of the beam section was implemented from the result in subsection 5.2.1 since the applied force will come from the piston pin and through the beam from the small end. It is also shaped very similar to the results from subsection 5.2.3, underlining the reason to copy this part of the result.

The front and back of the beam section when looking in the XY-plane where covered with triangular shaped extrudes to get a more H-rod shape on the conrod. These also implemented the result from subsection 5.2.4, and increased the stiffness of the rod.

The hollow sections were implemented to both Design 2.0 and 2.1 after having tested the non-hollow-beam designs statically in NX. This way material could be removed from the sections with the lower stresses, a process that was done iteratively for each hollow section.

6.2 Meshing

The mesh features used for the different connecting rods were decided based on the complexity of their geometry. For the traditional approach conrod an element size of 2.5 mm was chosen considering there were no tiny wholes and no features smaller than this in the internal geometry. This is also why the SCBSV was not set higher than 50. Given that the internal geometry had no edge blends and most of the corners were 90° it was decided that the small feature tolerance could remain at default 10% of the element size. The features are shown in Figure 5.6.

When meshing Design 2.0 and 2.1 a more complex geometry than the one in the traditional approach had to be taken into account. Both designs contained edges and internal holes that complicated the mesh. Multiple small geometrical features lead to an increase in SCBSV, as mentioned in subsection 5.3.4. Given the complexity of the internal geometry in Design 2.0 the mesh of this conrod should have a higher SCBSV and smaller SFT than Design 2.1. This is not the case here since any attempts of creating a more precise mesh either took way too long to mesh, or caused the mesh to fail. This lead the SFT to remain at 10%, and limited the SCBSV to 60% and the element size to 1.6 mm.

Design 2.1 on the other hand was easier to mesh with stricter mesh features, seen in the mesh features of the final mesh of this design in Figure 5.42. This due to its less complex internal geometry compared to Design 2.0. The SFT was set to 4% to get the highest accuracy of the stresses around the edge blends both in the internal geometry and the external parts of the beam section.

6.3 Static Analysis in NX

Comparing the stresses from the static analysis on the traditional approach conrod, seen in Figure 5.7, to the ones obtained in the semester project one can see that the quantity of critical stress points in the beam section has almost been reduced to zero. This indicates that a design with a bigger internal pattern significantly reduces the issue with the high stress concentration gatherings in the beam section. The maximum stresses of 802 MPa

found in the small end is marginally lower than the yield strength of the material, at 805 MPa. But given that these stresses will be alot lower when the forces are applied more correctly in FEDEM, they were not considered as worrisome at this point, neither was the maximum deformation.

Both Design 2.0 and Design 2.1 exceeded their yield strength in the static analyses performed on them, but were still not discarded. Design 2.0 had its maximum stresses in the small end just like for the traditional approach conrod, and as mentioned several times before, these would decrease when the loads are applied properly. The low stresses in the rest of the beam as well as a maximum deformation of only 308 μm were also a factor in approving this design for further analyses.

Design 2.1 had its maximum stresses located inside the throughgoing hole of the beam at an edge blend. Considering that the rest of the beam had stresses well below 750 MPa and the location of the stress concentration Design 2.1 was also approved for furter analyses. The maximum deformation also played a part, being 15 μm lower than for Design 2.0.

6.4 Stiffness Analysis

All of the new designs had a greater stiffness about the X-axis than the MXRR conrod, Design 2.1 having the lowest X-axis stiffness of the three; 250 mm^4 higher than for the OEM rod. This would lead to a greater resistance towards the "front-rear buckling and the catastrophic buckling" about the X-axis described by Strozzi et al. (2015). Non of the conrods show any unexpected drop in moment of inertia and the values are reasonably consistent throughout the beam section. When compared to the benchmark conrod, the biggest difference is found in the constancy in moment of inertia from sections three through twelve for the MXRR rod; The MXRR conrod graph, Figure 4.8, has a derivative of about zero for the beam section.

The moment of inertia about the Z-axis on the other hand is around 400 mm^4 lower for the traditional approach conrod and Design 2.0, while design has a moment of inertia 800 mm^4 lower than the OEM rod. This is over 20% lower which is significant, and a buckling analysis would be necessary to determine if the stiffness about the Z-axis is sufficient. This has not been done as time did not permit it.

6.5 FEDEM Analysis

The calculation of bob weights made it possible to implement the balancing masses in FEDEM, getting a more accurate result in the simulations by equalizing the inertial forces created by the non-centered masses about the center of rotation, such as the conrod, piston, etc. In a real engine these balancing masses also reduce vibration occurring during the reciprocating motion inside the engine block by moving the center of mass of the system as close as possible to its center of rotation. This is vital for the endurance and lifetime of the motor.

All three proposed designs have a higher Small end/Big end mass ratio than the OEM rod, but being between four and seven grams lighter than the OEM conrod they all have

lighter bob weights. Another result of the lighter weight is the maximum rpm achieved by the motor applied with the new designed conrods. An increase of over 400 rpm's is a significant improvement on the MXRR conrod. This improvement in performance is also shown in the maximum compression values of the conrods, lying between 60 and 120 μm lower than the compression of the OEM conrod.

The worrying part of the simulations is the values of the stress concentrations in all three conrods. The yield strength for the titanium selected for the AM process is 805 MPa. For the traditional approach conrod this could indicate that yielding occurs somewhere inside the conrod given that no stresses on the visible elements of the conrod exceed 600 MPa. As FEDEM has no way of looking inside the conrod, it will be impossible to know whether or not these high stresses are due to problems with the mesh or if they are real. A maximum stress value that close to the visible maximum on the beam make it more plausible that these stress concentrations are real rather than false.

Design 2.0 also has stress concentrations way above the yield stress of the material. A common denominator for all of them though is that they are located on sharp edges and that there is no symmetric response to these concentrations. This could indicate that these stress concentrations are false. In the actual design these edges are rounded off and there would be no reason to believe that would lead to a more dispersed distribution of stresses, and an avoidance of these stress concentration points. The fact that neighbouring elements and their twin elements mirrored about the axes of symmetry are not equally stressed further underlines that these stress concentrations may be false.

Just as for Design 2.0, Design 2.1 have some unsymmetrical stress concentration areas exceeding 900 MPa. In addition to this the symmetrical stresses around the connecting areas between the small end and big end reaching around 800 MPa are worrisome. More so than the unsymmetrical stresses since they don't occur on any of the three different mirrored areas about the different axes of symmetry. These concentrations can therefore most likely be considered as false.

6.6 Materials

There is no doubt that a titanium alloy is the material needed to produce these lightweight-high strength conrods, given their ability to endure higher stress amplitudes in HCF and their density being around 50% compared to most steel alloys. The material selected for this application is the Ti6Al4V, due to its ability to maintain most of its material properties compared to machined parts when its additively manufactured, using an SLM-method. DMLM is the method that gives the highest density possible of the AM methods looked at in this thesis, a crucial factor in avoiding the creation of porous structures in the finished part. Given that the HCF properties improve according to the improvement in Yield Strength by using the method described by Xu et al. (2017), this is the process ideal for the production of an AM conrod.

The biggest concern with the conrods designed and proposed in this thesis is the high stresses occurring in all three designs, almost reaching 900 MPa. With the properties of the super Ti6Al4V described by Xu et al. (2017), these conrods would no longer be in danger of yielding for the maximum stresses found in the analyses of this thesis. If the HCF life of this material is not satisfactory, the stress concentrations could be removed by

removing the internal hollow regions in the area where these occur. This would add mass to the beam section, most likely moving the center of mass closer to the small end, and zero out the advantages the new designs have on the OEM conrod, since this would effect the total mass, reducing the maximum rpm achieved.

6.7 Topology Optimization in NX 12.0

By looking at the result summary in Figure 6.1 it is not hard to argue that the designs achieved by using topology optimization have a lower performance than the traditional approach design. There could be several reasons for this, but having to approximate the load cycle of the rod using four different load cases is clearly a factor. The fact that the results from the simulations could neither be meshed or used directly did not help either. With a better approximation of the load cases and an easier way to use the results of the optimizations directly in the modeling application the results may have been better.

Chapter 7

Conclusion

This thesis has given a brief introduction on connecting rods, analyzed and reviewed state of art AM processes with regards to material properties and surface quality of four different metal alloys, as well as proposing three new designs for AM conrods with improved properties compared to the OEM conrod of MXRR. The designs were created using two different approaches, one of them implementing topology optimization resulting in organic structures that provided some interesting results.

The designs were tested in the FVTB and benchmarked up against each other using four KPI's described in Section 4.6, and a summary of the results was shown in Figure 6.1. The table shows that all designs proposed have better mechanical properties than the OEM conrod in all aspects except mass ratio and the minimum moment of inertia about the Z-axis. If the super Ti6Al4V described by Xu et al. (2017) has a HCF-life similar to the wrought and machined Ti6Al4V this material would be ideal for this application and would permit the production of these newly designed connecting rods. If not, the maximum stress concentrations would be too close to the material yield strength.

A better understanding of the Topology Optimization application in NX 12.0 could have provided better results from this approach, but from the result summary the traditional approach conrod is the design of choice. It would improve the OEM motor in all aspects except the stiffness about the Z-axis. Given that a buckling analysis does not determine its Z-axis stiffness as too low and that the SLM manufactured Ti6Al4V can achieve a good enough HCF-life, there is no reason why MXRR should not consider this conrod as a possible replacement for the OEM-rod. This is based solely on the KPI's of this thesis.

Further Work

In continuation of the research presented in this thesis a more profound stiffness analysis including buckling analysis would have to be performed. A HCF-life test of the SLM manufactured Ti6Al4V of Xu et al. (2017) would have to be executed and an altering of the balancing masses of the crankshaft would have to be done to match the new weight of the conrod.

Bibliography

AlMangour, B., Yang, J. M., 2016. Improving the surface quality and mechanical properties by shot-peening of 17-4 stainless steel fabricated by additive manufacturing, Table 3. Elsevier B.V.

Ek, R. K., Rännar, L. E., Bäckstöm, M., Carlsson, P., 2016. The effect of EBM process parameters upon surface roughness. Rapid Prototyping Journal 22 (3).

Fedem Technology AS, 2016. Fedem User's Guide. Fedem.

GE, 2018. Electron Beam Melting. Last accessed 10 of October 2018.
URL https://www.ge.com/additive/additive-manufacturing/information/electron-beam-melting-technology

Kuang-Hua, C., 2015. Design Theory and Methods Using CAD/CAE, Chapter 4.6. Elsevier.

Mower, T. M., Long, M. J., 2015. Materials science and engineering, pages 198-213. Elsevier B.V.

Rølvåg, T., Bella, M., 2017. Dynamic test bench for motocross engines. SAGE Journals 9 (1-19).

Siemens PLM Software Inc, 2014. Element library reference. Last accessed 15 of May 2019.
URL https://docs.plm.automation.siemens.com/data_services/resources/nxnastran/10/help/en_US/tdocExt/pdf/element.pdf

Strozzi, A., Baldini, A., Giacopini, M., Bertocchi, E., Mantovani, S., 2015. A repertoire of failures in connecting rods for internal combustion engines, and indications on traditional and advanced design methods. Elsevier B.V.

Vayssette, B., Saintier, N., Brugger, C., Elmay, M., Pessard, E., 2017. Surface roughness of Ti-6Al-4V parts obtained by SLM and EBM: Effect on the High Cycle Fatigue Life. Elsevier B.V.

Wills, G., 2017. Nx 12 topology optimization for designers. Last accessed 26 of April 2019.
URL https://www.plm-europe.org/admin/presentations/2017/2003_PLMEurope_24.10.17-13-30_GUY-WILLS_SPLMM_topology_optimization_for_designers.pdf

Xu, W., Lui, E., Pateras, A., Qian, M., Brandt, M., 2017. In situ tailoring microstructure in additively manufactured ti-6al-4v for superior mechanical performance. Elsevier.

Appendix

MATERIAL INFORMATION

Material : Titanium Ti-6Al-4V

Material properties: Referenced library material : physicalmateriallibrary.xml Library Version : 4.0 Material Type: Isotropic Label: 1 Alternate Name : Category : METAL Sub-Category : Titanium Alloy Mass Density (RHO) : 4.43e-06 kg/mm

======== Mechanical Young's Modulus (E) : 121000000 kPa : Major Poisson's Ratio Poisson's Ratio (NU) : 0.34 Shear Modulus (G) : Not defined Structural Damping Coefficient (GE) : Not defined Stress-Strain Input Data Type : Engineering Stress-Strain Stress-Strain (H) : Not defined Type of Nonlinearity (TYPE) : PLASTIC Yield Function Criterion (YF) : von Mises Hardening Rule (HR) : Isotropic Initial Yield Point (LIMIT1) : Not defined Initial Friction Angle (LIMIT2) : Not defined Mechanical Power to Heat Ratio : 0

======== Strength Yield Strength : 805000 kPa Ultimate Tensile Strength : 845000 kPa Tsai-Wu Interaction Coefficient (F12): Not defined Tension (ST) : Not defined Compression (SC) : Not defined Shear (SS) : Not defined Tension (XT) : Not defined Compression (XC) : Not defined Shear (XS) : Not defined

======== Durability Stress-Life Data : Expression Fatigue Strength Coefficient : 1293000 kPa Fatigue Strength Exponent : -0.088 Strain-Life Data : Expression Fatigue Ductility Coefficient : 0.26 Fatigue Ductility Exponent : -0.721 Cyclic Yield Strength : Not defined Cyclic Strength Coefficient : Not defined Cyclic Strain Hardening Exponent : Not defined Fatigue Limit Strength in Bending : Not defined Fatigue Limit Strength in Torsion : Not defined Percent Reduction in Area : 0 R-Ratio : Specify : -1 Test Type : Tension Survival Probability : 50 Tsigma (90/10) : 1.5 : Cycles Number of Cycles : Not defined

======== Formability Work Hardening : Not defined Forming Limit : Not defined Plastic Strain Ratio : Not defined Initial Strain : 0.02 mm/mm Hardening Exponent : 0.2 Strength Coefficient : 1449.277 MPa R0 : 1.4 R45 : 1.5 R90 : 1.7 Bend Radii - SI Material Stock : No Field Bend Radii - English Material Stock : No Field

======== Thermal/Electrical Temperature (TREF) : Not defined Thermal Expansion Coefficient (A) : 8.6e-06 C Thermal Conductivity (K) : 6700 W/(mmC) Specific Heat (CP) : 526000000 J/(kgK) Latent Heat (L) : Not defined Phase Change Temperature : Not defined Phase Change Temperature Range : Not defined Specific Heat Above Phase Change : Not defined Resistivity : Not defined Scattering : Not defined Extinction : Not defined Scattering : Not defined Extinction : Not defined

======== Creep : None

======== Viscoelasticity Model : None

======== Viscoplasticity Viscoplastic Type : None

======== Damage : None

======== Miscellaneous Fixed Stock Thickness : false Default Thickness : Not defined Adhesive : Adult HIC1000 Offset : Not defined Adult HIC1700 Offset : Not defined Child HIC1000 Offset : Not defined Child HIC1700 Offset : Not defined Leg Impact Offset : Not defined NCAP Adult 650 Offset : Not defined NCAP Child 650 Offset : Not defined NCAP Adult 1000 Offset : Not defined NCAP Child 1000 Offset : Not defined NCAP Adult 1350 Offset : Not defined NCAP Child 1350 Offset : Not defined NCAP Adult 1700 Offset : Not defined NCAP Child 1700 Offset : Not defined Crosshatch Pattern : Refractory

---

Material : Titanium MXRR

Parent Material : Titanium Ti-6Al-4V Parent Material Library : physicalmateriallibrary.xml Parent Material Library Version : 4.0

Material properties: Locally defined material Material Type: Isotropic Label: 4 Alternate Name : Category : METAL Sub-Category : Titanium Alloy Mass Density (RHO) : 4.43e-06 kg/mm

======== Mechanical Young's Modulus (E) : 110000000 kPa : Major Poisson's Ratio Poisson's Ratio (NU) : 0.34 Shear Modulus (G) : Not defined Structural Damping Coefficient (GE) : Not defined Stress-Strain Input Data Type : Engineering Stress-Strain Stress-Strain (H) : Not defined Type of Nonlinearity (TYPE) : PLASTIC Yield Function Criterion (YF) : von Mises Hardening Rule (HR) : Isotropic Initial Yield Point (LIMIT1) : Not defined Initial Friction Angle (LIMIT2) : Not defined Mechanical Power to Heat Ratio : 0

======== Strength Yield Strength : 862000 kPa Ultimate Tensile Strength : 960000 kPa Tsai-Wu Interaction Coefficient (F12): Not defined Tension (ST) : Not defined Compression (SC) : Not defined Shear (SS) : Not defined Tension (XT) : Not defined Compression (XC) : Not defined Shear (XS) : Not defined

======== Durability Stress-Life Data : Expression Fatigue Strength Coefficient : 1293000 kPa Fatigue Strength Exponent : -0.088 Strain-Life Data : Expression Fatigue Ductility Coefficient : 0.26 Fatigue Ductility Exponent : -0.721 Cyclic Yield Strength : Not defined Cyclic Strength Coefficient : Not defined Cyclic Strain Hardening Exponent : Not defined Fatigue Limit Strength in Bending : Not defined Fatigue Limit Strength in Torsion : Not defined Percent Reduction in Area : 0 R-Ratio : Specify : -1 Test Type : Tension Survival Probability : 50 Tsigma (90/10) : 1.5 : Cycles Number of Cycles : Not defined

======== Formability Work Hardening : Not defined Forming Limit : Not defined Plastic Strain Ratio : Not defined Initial Strain : 0.02 mm/mm Hardening Exponent : 0.2 Strength Coefficient : 1449.277 MPa R0 : 1.4 R45 : 1.5 R90 : 1.7 Bend Radii - SI Material Stock : No Field Bend Radii - English Material Stock : No Field

======== Thermal/Electrical Temperature (TREF) : Not defined Thermal Expansion Coefficient (A) : 8.6e-06 C Thermal Conductivity (K) : 6700 W/(mmC) Specific Heat (CP) : 526000000 J/(kgK) Latent Heat (L) : Not defined Phase Change Temperature : Not defined Phase Change Temperature Range : Not defined Specific Heat Above Phase Change : Not defined Resistivity : Not defined Scattering : Not defined Extinction : Not

defined Scattering : Not defined Extinction : Not defined

======== Creep : None

======== Viscoelasticity Model : None

======== Viscoplasticity Viscoplastic Type : None

======== Damage : None

======== Miscellaneous Crosshatch Pattern : Refractory Fixed Stock Thickness : false Default Thickness : Not defined Adhesive : Adult HIC1000 Offset : 95 mm Adult HIC1700 Offset : 74 mm Child HIC1000 Offset : 85 mm Child HIC1700 Offset : 68 mm Leg Impact Offset : 50 mm NCAP Adult 650 Offset : 115 mm NCAP Child 650 Offset : 105 mm NCAP Adult 1000 Offset : 94 mm NCAP Child 1000 Offset : 90 mm NCAP Adult 1350 Offset : 74 mm NCAP Child 1350 Offset : 70 mm NCAP Adult 1700 Offset : 65 mm NCAP Child 1700 Offset : 60 mm

Mesh quality Traditional Approach Conrod:

========== Results of Element Shape Check ==========

Overview

Number Failed Number Warning Number Checked Elements 243 61 22943

Check Number Failed Number Warning Worst Value Jacobian Sign 0 0 1.000000 Jacobian Zero 0 60 0.007498 Volume 0 7 0.005986 Axisymmetric 0 0 -N/A- Consistent Y Axisymmetric +X 0 0 -N/A- Aspect Ratio 0 1 10.291448 Skew Angle 0 0 -N/A- Maximum Interior 0 0 -N/A- Angle Minimum Interior 0 0 -N/A- Angle Taper 0 0 -N/A- Warp Factor 0 0 -N/A- Face Warp 0 0 -N/A- Coefficient Edge Point 243 0 79.822612 Included Angle Edge Point Length 0 0 0.699504 Ratio Element Offset 0 0 -N/A- Length Ratio

Mesh quality Design 2.0:

========== Results of Element Shape Check ==========

Overview

Number Failed Number Warning Number Checked Elements 2504 11690 413842

Check Number Failed Number Warning Worst Value Jacobian Sign 0 0 1.000000 Jacobian Zero 0 11690 0.000110 Volume 0 2636 0.000033 Axisymmetric 0 0 -N/A- Consistent Y Axisymmetric +X 0 0 -N/A- Aspect Ratio 0 4 20.071949 Skew Angle 0 0 -N/A- Maximum Interior 0 0 -N/A- Angle Minimum Interior 0 0 -N/A- Angle Taper 0 0 -N/A- Warp Factor 0 0 -N/A- Face Warp 0 0 -N/A- Coefficient Edge Point 2504 0 84.802520 Included Angle Edge Point Length 0 3 0.598614 Ratio Element Offset 0 0 -N/A- Length Ratio

Mesh quality Design 2.1:

========== Results of Element Shape Check ==========

Overview

Number Failed Number Warning Number Checked Elements 575 58527 206218

Check Number Failed Number Warning Worst Value Jacobian Sign 0 0 1.000000 Jacobian Zero 0 58527 0.000087 Volume 0 31288 0.000050 Axisymmetric 0 0 -N/A- Consistent Y Axisymmetric +X 0 0 -N/A- Aspect Ratio 0 6 11.361534 Skew Angle 0 0 -N/A- Maximum Interior 0 0 -N/A- Angle Minimum Interior 0 0 -N/A- Angle Taper 0 0 -N/A- Warp Factor 0 0 -N/A- Face Warp 0 0 -N/A- Coefficient Edge Point 575 0 78.130418 Included Angle Edge Point Length 0 4 0.546623 Ratio Element Offset 0 0 -N/A- Length

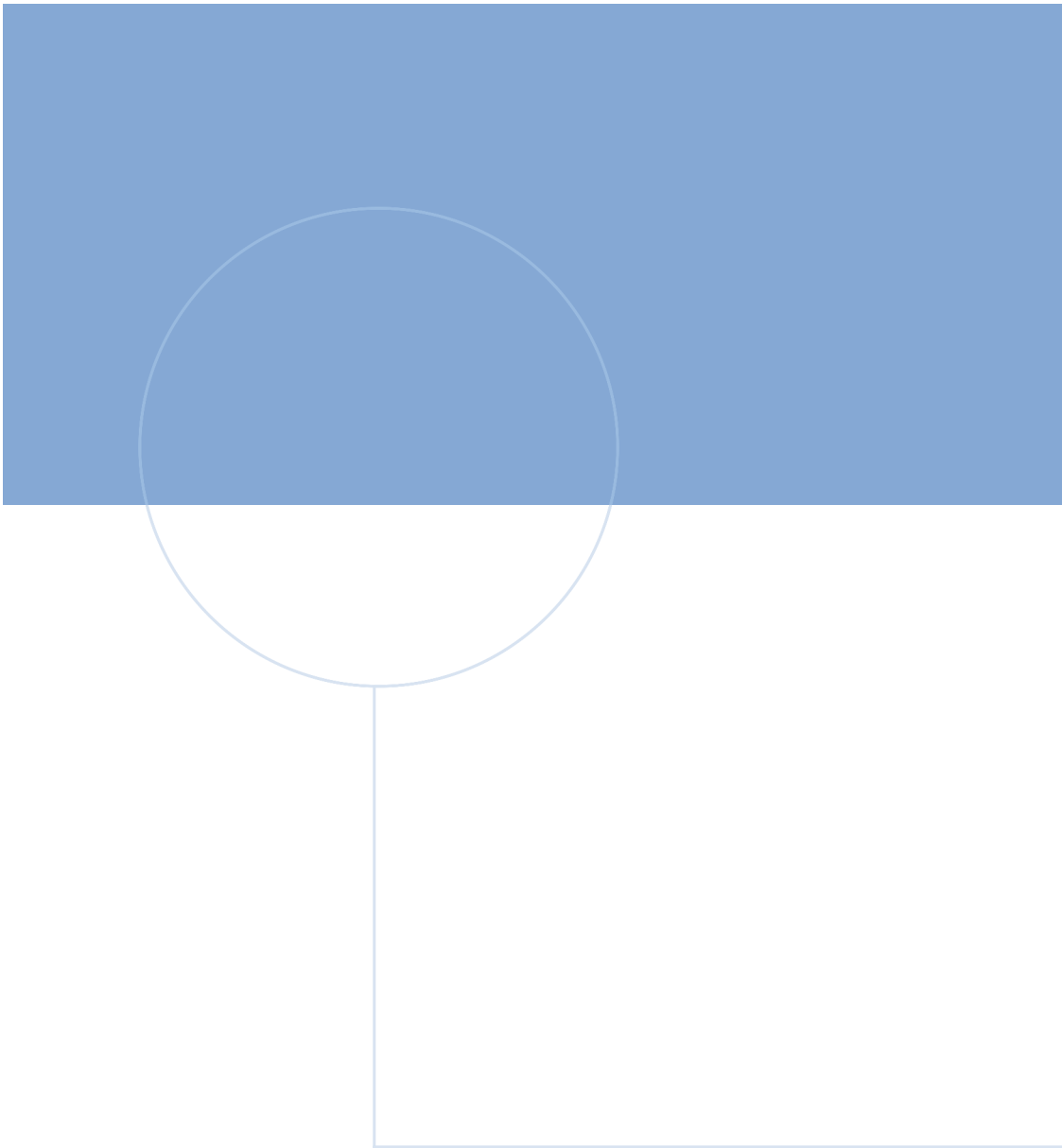

NTNU

Kunnskap for en bedre verden